OPTIMAL RE-ENTRY TRAJECTORY TERMINAL STATE DUE TO VARIATIONS IN WAYPOINT
LOCATIONS

THESIS

William J. Karasz

AFIT/GA/ENY/08-D01

DEPARTMENT OF THE AIR FORCE
AIR UNIVERSITY

AIR FORCE INSTITUTE OF TECHNOLOGY

Wright-Patterson Air Force Base, Ohio

AFIT/GA/ENY/08-D01

OPTIMAL RE-ENTRY TRAJECTORY TERMINAL STATE DUE TO VARIATIONS IN WAYPOINT LOCATIONS

THESIS

Presented to the Faculty

Department of Aeronautics and Astronautics

Graduate School of Engineering and Management

Air Force Institute of Technology

Air University

Air Education and Training Command

In Partial Fulfillment of the Requirements for the

Degree of Master of Science

William J. Karasz, B.S.E.S.

DAGSI

December 2008

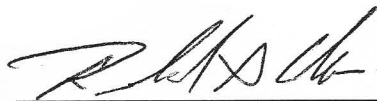APPROVED FOR PUBLIC RELEASE; DISTRIBUTION UNLIMITED.

AFIT/GA/ENY/08-D01

OPTIMAL RE-ENTRY TRAJECTORY TERMINAL STATE DUE TO VARIATIONS IN WAYPOINT
LOCATIONS

William J. Karasz, B.S.E.S.

DAGSI

Approved:

_____   _____
Dr. Richard G. Cobb (Chairman)   Date   11 Dec 08

_____   _____
LtCol Kerry D. Hicks (Member)   Date   12 Dec 08

_____   _____
Dr. William P. Baker (Member)   Date   12 Dec 08

AFIT/GA/ENY/08-D01

Abstract

The Air Force's Prompt Global Reach concept describes the desire to have a capability to reach any target within a 9000 nautical mile distance within two hours of launch. To meet this objective, much effort is being devoted to hypersonics and re-entry vehicles. A hypersonic vehicle typically has poor aerodynamic efficiency, and therefore, can only make small alterations to its trajectory. Given the limited maneuverability, computational modeling is used to generate trajectories before launch to strike intended targets. In addition to endpoint (target) constraints, waypoints may be necessary for reconnaissance, multiple payloads, or other logistical activities. Once the optimal trajectory is solved to satisfy the endpoint and waypoint constraints, the next question asked is, "Where else can the vehicle go while still meeting the mission objectives, and what is the penalty for making such maneuvers?" The result of this research is a direct numerical solution technique for mapping the sensitivity of the terminal state as a function of additional waypoint location while satisfying vehicle dynamics, control limitations, and all previously defined waypoint constraints. Multiple cases are presented including a simple endpoint-to-endpoint scenario and a waypoint included scenario, with a Gauss pseudospectral solver as the direct numerical solver.

iv

Acknowledgements

I would like to express my sincere appreciation to my faculty advisor, Dr. Cobb, for his guidance and support throughout the course of this thesis effort, and to my loving fiancée who provided endless encouragement and support.

William J. Karasz

Table of Contents

List of Figures

List of Tables

List of Symbols

t, τ dimensional, non-dimensional time

t_0, τ_0 dimensional, non-dimensional initial time

t_f, τ_f dimensional, non-dimensional final time

$x(t)$ state vector

$u(t)$ control vector

J cost function

ϕ terminal constraint

r' non-dimensional radius

$^R V'$ non-dimensional relative velocity

θ' non-dimensional longitude

ϕ' non-dimensional latitude

γ' non-dimensional flight-path-angle

ψ' non-dimensional heading angle

m number of path constraints or vehicle mass

n number of states

p number of event constraints (boundary conditions)

λ costate Lagrange multiplier

H Hamiltonian

$\sigma_{min}, \sigma_{max}$ minimum/maximum bank angle

C_L coefficient of lift

C_D coefficient of drag

C_L^* coefficient of lift that produces the maximum lift-to-drag ratio

c_l fraction of C_L^*

E lift-to-drag ratio or aerodynamic efficiency

E^* maximum lift-to-drag ratio

β atmospheric scaling height

$\omega_\oplus , \omega_\oplus'$ dimensional, non-dimensional rotation rate of Earth

S wetted surface area

B $\dfrac{\rho_0 S C_L^* r_0}{2m}$, grouped terms of vehicle parameters and reference conditions

ρ_0 atmospheric density at radius r_0

r_0 reference radius

List of Abbreviations

Abbreviation
CAV   Common Aero Vehicle
CONOPS   Concepts of Operation
DARPA   Defense Advanced Research Projects Agency
EOM   Equation of Motion
FALCON   Force Application Launch from Continental United States
FASST   Flexible Aerospace System Solution for Transformation
GPM   Gauss Pseudospectral Method
GPOCS   Gauss Pseudospectral Optimal Control Software
GPOP   Gauss Pseudospectral Optimal Program
GPA   Global Persistent Attack
GS   Global Strike
HCV   Hypersonic Cruise Vehicle
HBVP   Hamiltonian boundary-value problem
IPOPT   Interior Point Optimizer
LPM   Lobatto Pseudospectral Method
LRGPE   Long Range Global Precision Engagement
NASA   National Aeronautics and Space Administration
NGLT   Next Generation Launch Technology
NLP   Non-linear Program
OPENPOCS   Open Pseudospectral Optimal Control Software
PSCOL   Pseudospectral Collocation
RLV   Reusable Launch Vehicle
RV   Re-entry Vehicle
RPM   Radau Pseudospectral Method
USAF   United States Air Force
w.r.t.   With Respect To

OPTIMAL RE-ENTRY TRAJECTORY TERMINAL STATE DUE TO VARIATIONS IN WAYPOINT LOCATIONS

I. Introduction

1.1 Motivation

The United States Air Force's Concept of Operations (CONOPS) includes Global Strike (GS) and Global Persistent Attack (GPA). These concepts are the result of an Air Combat Command study conducted in 2002, in which the United States Air Force (USAF) queried the industry about which technologies and research would be needed to have a Long Range Global Precision Engagement (LRGPE). "The key focus area is on the capability to strike targets anywhere and anytime within the global battlespace…"[1]. The key focus was further refined to include the element of time. Therefore, research is being dedicated to hypersonic and re-entry vehicles capable of engaging any target on the Earth within 12 hrs, i.e. Prompt Global Strike.

A more recent progress report on where the United States stands in terms of Prompt Global Strike was given by General Chilton in his statement to the House Armed Services Committee on 27 February 2008 [14]. He states that we have a "Prompt global strike capability on alert today, but it is configured only with nuclear weapons." Nuclear weapons have a large range of destruction that may include assets we wish to protect, thereby precluding this option as a means of deterrence. General Chilton goes on to say, "The capability we lack is the means to deliver prompt, precise, conventional kinetic effects at inter-continental ranges. The ability to hold at risk sites in otherwise denied territory is a key element of our strategic deterrent capability." This is a gap in

the United States deterrent capability that is receiving high levels of interest and attention for a near-term solution [14].

The motivation highlighted above addresses the terminal objective of GS and GPA, but another facet of the problem involves optimal trajectory generation. The targets are considered to be time critical, therefore the wish is to minimize the time of flight to target. However, there are constraints to be considered such as political boundaries and borders, physical obstacles like mountains, and the desire to fly over specific waypoints for multiple payload departure points, communication relay, and other tasks. Coupled with these tasks are the limitations of the vehicle: vehicle dynamics, heating constraints, g load, etc.

In addition to the military needs cited above, NASA's Integrated Space Transportation Plan/Program (ISTP) seeks to expand the civil and commercial reach into space for the coming decades [5]. This plan emphasizes Reusable Launch Vehicles (RLV). Presently, there are two general thoughts for retrieving RLVs, either recover the RLV downrange of the launch site and transport it back to the launch facility or fly/glide the RLV back to the launch site. The latter option is preferred since it does not require off-site resources to recover the vehicle, and the vehicle can otherwise land and be serviced immediately for a quick turn-around time.

1.2 Problem Description

The long-term goal of this research is to provide a tool to mission strategists capable of providing near real-time feedback of all feasible waypoints given an initial condition and final target. Such a scenario faced by a strategist would include identifying a finite number of targets or waypoints, determining if the waypoints are

feasible, and evaluating the associated costs. The choice of one waypoint will reduce the subset of further feasible waypoints, and this process will continue until the subset of remaining feasible waypoints is zero. A trajectory minimizing the time to final target will determine how the RV maneuvers between discrete waypoints.

In hypersonics, it is somewhat commonly known that small deviations off the nominal trajectory can throw the vehicle significantly off course. The same is true if the trajectory is purposely modified to move a waypoint or avoid a no-fly zone. Therefore, the type of problem to be addressed herein is a sensitivity analysis to waypoint location. Although closely related to perturbation and uncertainty theory, sensitivity theory is interested in characterizing changes in some parameter with respect to a specific event. In particular, the effects on terminal state with respect to changes in waypoint location will be investigated.

In summary, the goals of this research are to:

Use a high fidelity simulation of a hypersonic re-entry vehicle with a fixed initial condition and preselected final target position to:

a. *Determine a minimum time flight trajectory satisfying all imposed vehicle constraints.*

b. *Investigate the sensitivity on the primary mission objective (time to target) as the number and location of intermediary waypoints are imposed on the trajectory.*

In addition to the above goals, this research intends to increase the model fidelity for a more realistic simulation. In general, simplified assumptions in the model dynamics are justified by the need for comparatively short computational time. The decision to make simplifications to the model dynamics must be balanced with accuracy and minimizing error. To illustrate, imagine a compass onboard a ship in the open ocean that has an accuracy of $\pm 1°$. As the ship approaches a course heading change, the

3

magnitude of the heading change only needs to be known to the nearest degree since the compass is only good to $\pm 1°$. However if the ship must navigate through narrow channels or risk running aground, then both the compass accuracy and required heading change need to be known with greater precision. Two different types of compasses could be used for each of the applications; i.e., one compass that uses the magnetic field lines with a correction based on location for a quick but not as precise heading, while the other compass uses a GPS system which requires a few seconds to calculate the heading based on the difference between the ship's present position, to its position ten seconds prior. Hypersonic vehicles can be likened to the ship navigating through narrow channels, and requiring, therefore, precise navigation. The previous work upon which this research is built used a simplified dynamics model that, while unrealistic, nevertheless proved useful in analysis of an optimal trajectory. Therefore the second goal of this research is to:

Apply high fidelity 3-D dynamics, the results of which may be compared with results derived using the simplified model.

The challenge to finding an optimal re-entry trajectory in general is further complicated by vehicle control limitations, material properties, and human limitations. Such restrictions are applied to ensure a survivable trajectory for both the vehicle and crew, if manned. Figure 1 below shows the flight corridor for the space shuttle with two different models. The graphic on the left is from the flight test program, and on the right is the operational angle-of-attack profile. Although the pre-computed trajectory may satisfy the computer model dynamics, it may violate the operational constraints.

Accounting for all dynamics and constraints in trajectory generation becomes important for vehicle (and crew) survival.
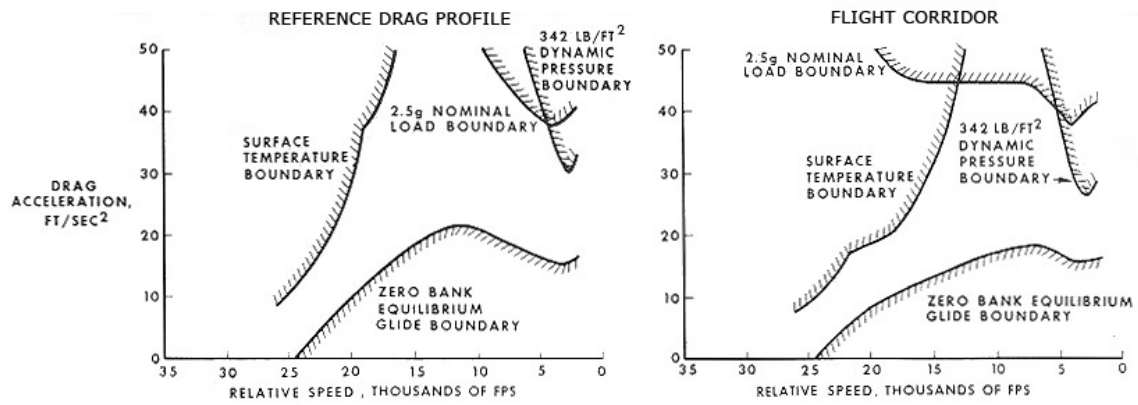
Figure 1. Shuttle Entry - Angle-of-Attack Profiles [18].

II.   Previous Research

This research extends the research carried out by Maj. Jorris [23]. His research

provided a "synergistic solution encompassing three key technologies; trajectory

generation, waypoint satisfaction, and threat or no-fly zone avoidance." His solution

used a Gauss Pseudospectral Method (GPM) form of dynamic optimization. His

technique lays out the groundwork for solving the optimal trajectory, but it is only part

of the research required to tackle this new problem. The other key area of research

addresses the solution sensitivity to changes in mission parameters and incorporates a

spherical Earth model and its rotation.

2.1   Dynamic Optimization

Dynamic optimization has the goal of finding the optimal control variables such

that an objective function, J, is minimized or maximized without violating state

dynamics, boundary conditions, and equality and/or inequality path constraints. The

general optimal control problem is posed below.

Minimize

$$J = \Phi\left(x(t_0),t_0,x(t_f),t_f\right) + \int_{t_0}^{t_f} L\left(x(t),u(t),t\right)dt \tag{2.1}$$

subject to the dynamic constraints

$$\dot{x}(t) = f\left(x(t),u(t),t\right) \tag{2.2}$$

the event constraints (boundary conditions)

$$\phi\left(x(t_0),t_0,x(t_f),t_f\right) = 0 \tag{2.3}$$

and the path constraints

$$C\left(x(t),u(t),t\right) \leq 0 \tag{2.4}$$

where

$$x \in C\left(\mathbb{R}^n\right)$$
$$\phi \in \mathbb{R}^p \qquad (2.5)$$
$$C \in C\left(\mathbb{R}^m\right)$$

and n, p, and m are the number of states, event constraints and path constraints respectively.

This type of problem has been addressed from many angles. For simple problems, analytical solutions have been obtained and for others only numerical solutions exist. Numerical methods for solving the optimal control problem are solved via indirect or direct methods. The indirect method is characterized by formulating the first-order optimality conditions from the objective function and constraints and then solving the resulting Hamiltonian boundary value problem. In contrast, the direct method parameterizes the functions using function approximation, and transcribes the optimal control problem to a nonlinear programming problem. The next section examines some of the techniques used to solve dynamic optimal control problems.

2.1.1 Calculus of Variations

The Calculus of Variations or Method of Lagrange multipliers is an indirect method in which the dynamics and constraints are adjoined to the performance index with a time varying Lagrange multiplier, $\lambda(t)$. The new cost function then takes the form:

$$\bar{J} = \Phi\left(x\left(t_0\right), t_0, x\left(t_f\right), t_f\right) + \int_{t_0}^{t_f} \left[L\left(x(t), u(t), t\right) + \lambda^T(t) f\left(x(t), u(t), t\right) - \dot{x}(t)\right] dt \qquad (2.6)$$

A stationary solution exists when $d\bar{J} = 0$ for arbitrary $du(t)$. In other words the cost is either at a minimum, maximum or inflection point, and the formulation of the cost function determines which extreme has been found. From calculus of variations we get the Euler-Lagrange equations which are the first-order necessary conditions for a stationary solution to Equation (2.1) and (2.6) [11].

$$\dot{\lambda}(t) = -\frac{\partial H^T}{\partial x} \equiv -\frac{\partial L^T}{\partial x} - \frac{\partial f^T}{\partial x}\lambda \tag{2.7}$$

with boundary conditions

$$\lambda^T(t_f) = \frac{\partial \phi}{\partial x}(t_f) \tag{2.8}$$

where

$$H\big(x(t),u(t),\lambda(t),t\big) \triangleq L\big(x(t),u(t),t\big) + \lambda^T(t) f\big(x(t),u(t),t\big) \tag{2.9}$$

and a stationary solution exists if the optimality criterion is satisfied:

$$\frac{\partial H}{\partial u} = 0, \ t_0 \le t \le t_f \tag{2.10}$$

The problem reduces to a Two-Point Boundary-Value Problem (TPBVP) where the initial state and final Lagrange multipliers are known. The optimal solution is obtained using a 'shooting' algorithm by integrating the states forward in time and then integrating the Lagrange multipliers backward in time. The resultant Lagrange multipliers are called costates. The costates and state history are then used to extract the required control input. This method has a "small radii of convergence," and the solution may become unstable and diverge while either integrating the states forward or integrating the Lagrange multipliers backwards [26]. For convergence, this method

requires a good initial guess for the solution, which in some circumstances is difficult to obtain.

It is also possible to employ algorithms that look at the gradient of the dynamics and the performance function. Algorithms like Steepest Descent and other variations on following the gradient to a minimum are prone to only finding the local minimum. In the same vein, linearization provides a means of determining optimality about the point of expansion.

2.1.2 Karush-Kuhn-Tucker (KKT) Conditions

As a generalization to the method of Lagrange multipliers, Karush, Kuhn, and Tucker came up with necessary and sufficient conditions for optimal solutions, $x^{\circ}(t)$ where the superscript 'o' denotes optimal [12, 15, 16].

The conditions are:

1. $x^{\circ}(t)$ is feasible

2. There exist $\lambda(t)$ such that:

$$
\begin{aligned}
\nabla J\left(x^{\circ}\right) &= \lambda(t)\nabla C\left(x^{\circ}\right) \\
\lambda(t)C\left(x^{\circ}\right) &= 0 \\
\lambda(t) &\leq 0
\end{aligned}
\tag{2.11}
$$

The KKT conditions provide the fundamental tie between the indirect and direct methods.

2.1.3 Sequential Quadratic Programming (SQP) Methods

Sequential Quadratic Programming is an iterative method in which the quadratic problem is solved at each iteration. Solving the quadratic problem at each iteration will define a step towards the next search direction until the optimal solution is found. A

quadratic problem consists of a quadratic model of the cost function and linearized

constraints. The robustness and fast convergence of SQP methods has led to its

incorporation into many commercial Nonlinear Program (NLP) solvers such as the

industry standard Sparse Nonlinear Optimizer (SNOPT) from Stanford [17].

2.1.3.1 Nonlinear Programming (NLP)

Nonlinear programming refers to a specific class of dynamic optimization

problems in which the objective function and/or constraints are nonlinear and has the

form:

$$
\begin{aligned}
\min \quad & f(z) \\
\text{s.t.} \quad & g(z) \leq 0 \\
& h(z) = 0 \\
& z \in Z
\end{aligned}
\tag{2.12}
$$

where f is the objective/cost function to be minimized, g is the inequality constraints,

and h is the equality constraints. z is a vector of parameters that exist in the domain of

Z.

Such problems often require the equations to be discretized and processed in a

computer algorithm. The name 'program' in nonlinear programming refers to its

dependence on software. Numerous NLP solvers exist such as SNOPT, NPSOL, and

Interior Point Optimizer (IPOPT). Each of the solvers has unique features that make

them more or less attractive depending on the problem considered. SNOPT "employs a

sparse SQP algorithm with limited-memory quasi-Newton approximations to the

Hessian or Lagrangian," whereas NPSOL employs a dense SQP algorithm [4]. Both

SNOPT and NPSOL are effective for large-scale nonlinear problems whose functions

and gradients are computationally expensive to evaluate [4]. IPOPT implements an interior point method for solving large-scale nonlinear optimization.

2.1.4 Pseudospectral Methods

Pseudospectral methods are a direct method of solving the optimal control problem. The continuous differential equations are discretized and transcribed to a NLP and solved by one of many available NLP solvers. More specifically, it is a form of direct collocation where the state and its derivative are both determined at a finite number of points. The problem is divided into segments or phases and the state is approximated over each segment. A sample schematic of segment or phase linkages is shown in Figure 2. Phases can be connected in any order and may have multiple adjoining phases. The approximation is differentiated and must match the true function derivative at a finite number of points to satisfy the collocation conditions and ensure a smooth connection between the phases [26].
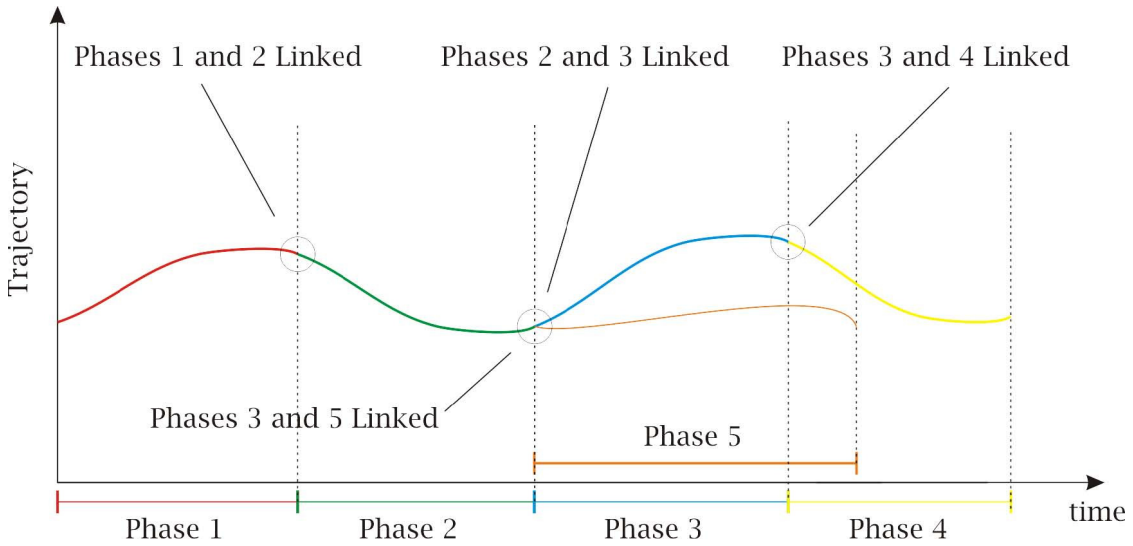
Figure 2. Schematic of linkages for multiple-phase optimal control problem [25].

The states are approximated using one of three collocation schemes, which is also the primary distinguishing feature between the various pseudospectral methods. The three collocation schemes are Lobatto, Radau, and Gauss. Lobatto collocation schemes impose the collocation condition at both endpoints. Examples of this method are Trapezoidal (order 2) and Hermite-Simpson (order 4) quadratures. Radau collocation schemes impose the collocation condition at only one end of the interval. Gauss schemes impose the collocation conditions strictly interior to the interval, of which the simplest Gauss collocation scheme is the midpoint rule [9].

Each of the segments contains a finite number of collocation points or nodes. The collocation points are usually the roots of an orthogonal polynomial although this is not a strict requirement. By choosing nodes that are roots of an orthogonal polynomial, the nodes become spaced in such a way that the Runge phenomenon is suppressed. The roots of differing degree polynomials are unique (except at zero and the endpoints) thereby ensuring uniform coverage over the interval of interest. The nodes and segments (state approximations) are then tied together using Lagrange polynomials. The theory behind pseudospectral methods is well documented in [22, 27].

There are a few software packages that integrate directly into MATLAB, such as DIDO and GPOCS, which use pseudospectral methods to solve the nonlinear optimal control problem. DIDO, written by I. Michael Ross, uses the Legendre-Gauss-Lobatto pseudospectral method or Lobatto Pseudospectral Method (LPM) [29]. DIDO is a software package that was initially used by Maj. Jorris in his analysis of the maneuvering re-entry vehicle, but Maj. Jorris later switched over to Gauss Pseudospectral Optimal Control Software (GPOCS) written by Anil Rao [25]. GPOCS

uses the Legendre-Gauss pseudospectral method or Gauss Pseudospectral Method

(GPM). The switch from DIDO to GPOCS was in part due to the availability of costate

and Hamiltonian information output by GPOCS that directly mapped to the Lagrange

multipliers. This was a key feature that Maj. Jorris used to verify the optimality of the

results for this class of problems. In his problem, and the one researched herein, the

Hamiltonian of the optimal solution is equal to a constant.

$$H = -1 \tag{2.13}$$

Figure 3 shows the equivalence of direct and indirect methods using the Gauss

pseudospectral discretization. The upper left box begins with a definition of the

continuous-time optimal control problem such as that presented in Section 2.1. Using an

'indirect' method requires formulating the first-order optimality conditions, and then

solving the resulting Hamiltonian boundary-value problem (HBVP). A 'direct' method

parameterizes the functions using function approximation, and then transcribes the

optimal control problem to a nonlinear programming problem (NLP) to solve for the

parameters. The equivalence of the two solution methods are then shown to be equal by

using the costate mapping theorem. The theory behind Gauss Pseudospectral methods

can be found in [22, 25] and has origins in Reddien's paper in SIAM Journal on Control

and Optimization [26].
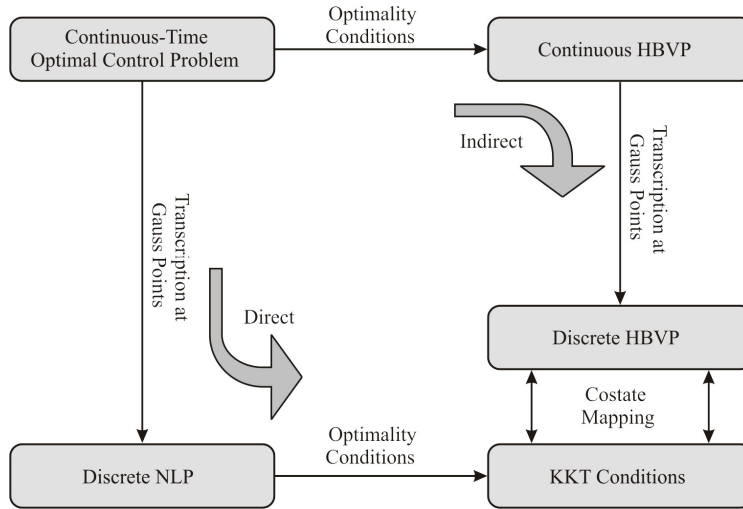
Figure 3. Equivalence of indirect and direct forms using the Gauss pseudospectral discretization [25].

Much of this research builds on the previous work of Maj. Jorris' dissertation, [23]. He demonstrated and proved that a direct collocation method such as that used in pseudospectral methods could be used to find optimal solutions for the re-entry problem considered herein. The pseudospectral method is not specific to a particular application such as re-entry trajectory generation, rather it is a method to find an optimal solution.

2.1.5   *Classical and Modern Control Methods (Inner-loop Control)*

Although not addressed by this research, once a trajectory is obtained, the task of following the optimal trajectory rests on the inner-loop controller. The inner-loop controller may include a human being or, for the autonomous system, a microprocessor alone. The optimal trajectory supplied by dynamic optimization methods is only as good as the inner-loop control tracking the reference trajectory. Inner-loop control tracking systems include models of the dynamics that are used to estimate the state and provide controls to drive the error between the desired trajectory and estimated

14

trajectory to zero. Extensive literature and examples exist for linear systems to track an

input; however, many of the techniques associated with linear systems cannot be

applied to the nonlinear re-entry problem. The solution is to transform the nonlinear

equations into linear equations so that the well developed linear tools can be used.

Methods for transforming the problem can be found in [30]. For this research, the

availability of suitable inner-loop control is assumed.

2.2   *Sensitivity Methods*

"The objective of sensitivity analysis is to quantify the effects of parameter

variations on calculated results" [13]. This research seeks to characterize how changes in

waypoint location affect the terminal state (the primary mission). Different techniques

and theories are considered for applicability to solving this problem. Included in the

review of sensitivity methods are perturbation, sensitivity, uncertainty theory, and a

direct approach. Particular caution is needed because there are subtle differences

between perturbation, sensitivity, and uncertainty analysis, and often these terms gets

mixed in the literature.

2.2.1   *Perturbation and Sensitivity Theory*

The traditional use of perturbation and sensitivity theory is to characterize the

stability of a system in the presence of perturbations or disturbances.   In general there

are three basic system responses: the system goes unstable; the system reacts to the

disturbance, but remains stable; or the system is unaffected by the disturbance. A

simple example is the pendulum, which exhibits both a stable and unstable mode. The

classic pendulum with friction when subjected to a disturbance will eventually settle

back to its stable equilibrium point, and the inverted pendulum will move away from

the equilibrium point due to the presence of any disturbances. This stability theory, however, while noted, is not the primary concern of this research, nor what is specifically sought after.

2.2.2   Uncertainty Analysis

"The objective of uncertainty analysis is to assess the effects of parameter uncertainties on the uncertainties in calculated results" [13]. In other words, uncertainty analysis is the study and characterization of a system where noise has been added to the system. This is an important aspect in inner-loop control, but trajectory generation deals in absolutes precluding this as an option.

2.2.3   Direct Approach

The direct approach is the oldest and most basic tool used in sensitivity analysis. It is also the least efficient as it requires solving the optimal control problem repeatedly over the variations or perturbations of interest. Due to the inapplicability of the previous methods, this method serves as the primary tool in this research. The direct approach is sufficient for mapping the sensitivity of an optimal control, but it is also the most computationally intensive.

2.3   3-D Dynamics Model and Fidelity

The previous research, from which this investigation is derived, used a 3-D dynamics model with the following assumptions [23]:

1. Flat, non-rotating Earth.

2. Gravity is constant.

3. Flight-path angle is small.

4. Drag is the dominant deceleration term.

5. Coefficient of Lift (C_L) and Coefficient of Drag (C_D) are functions of angle-of-attack only.

Using the above assumptions, the 3-D equations of motion are:

$$\dot{x} = V \cos\theta \tag{2.14}$$

$$\dot{y} = V \sin\theta \tag{2.15}$$

$$\dot{h} = V\gamma \tag{2.16}$$

$$\dot{V} = -\frac{BV^2 e^{-\beta r_0 h}\left(1 + c_l^2\right)}{2E^*} \tag{2.17}$$

$$\dot{\gamma} = BVe^{-\beta r_0 h} c_l \cos\sigma - \frac{1}{V} + V \tag{2.18}$$

$$\dot{\theta} = BVe^{-\beta r_0 h} c_l \sin\sigma \tag{2.19}$$

where x and y are lateral displacements, h is altitude, V is velocity, γ is flight-path-angle, and θ is heading. And the terms on the right-hand side of the equal sign: B is a grouping of vehicle parameters and initial conditions, σ is bank angle, c_l is the fraction of C_L^* (coefficient of lift that results in the maximum lift-to-drag ratio), E^* is the maximum lift-to-drag ratio, β is the atmospheric scaling height, and r_0 is a reference radius. The derivation and further explanation of the terms in the equations can be found in [23].

The assumptions above are suitable for:

1. A short duration trip where the rotation of the Earth is not a significant factor.

2. A short range trip where the curvature of the Earth is not a significant factor.

3. Shallow flight-path angle whereby gravity does not significantly change.

4. A vehicle that does not have retro firing thrusters or similar braking forces.

The assumptions above were used not for accuracy in modeling reality, but for simplifying the dynamics such that analytical solutions can be obtained and compared to the numerical results. Since this research looks to increase the model fidelity, the assumptions presented above will, in the majority, be modified. The flat Earth will be replaced with a spherical Earth. Rotation of the Earth will be turned back 'on.' Gravity will follow an inverse square law as a function of radial distance from the center of the Earth. Drag will remain the dominant deceleration term. The only assumption above that will be simplified further is that the coefficient of lift and drag will be held constant. In general, coefficients of lift and drag are a function of angle-of-attack, but they are held constant to simplify the control to one variable (bank angle).

2.4   Highlighted Vehicles

Although the recent GS and GPA concepts are motivating new hypersonic research, it is important to acknowledge the contributions from past and current contributions of hypersonic vehicles. Before delving into vehicle specifics, some classic definitions follow in the next section.

2.4.1   Vehicle Descriptors

The current buzzwords or acronyms describing hypersonic vehicles are CAV, HCV, and RLV. The terms change over time, but the underlying concepts remain the same. The definition of each term is now presented.

2.4.1.1 Common Aero Vehicle (CAV)

The Common Aero Vehicle (CAV) is a concept which describes a space re-entry aeroshell launched into space on a suitable vehicle, which then survives atmospheric re-entry, reduces its speed to low Mach numbers or even sub-Mach, and dispenses a cargo payload or weapon in the Earth's atmosphere. The conceptual CAV might be propelled into space by any of a number of present or future launch platforms and dispense a wide

variety of cargoes, payloads or weapons. Development of the CAV capability will satisfy future requirements enunciated in numerous national visions, future studies, and military plans and will ultimately be necessary to fully realize the opportunities inherent in operating from, through, and in space and give true meaning to the phrases global reach, global power projection, and global engagement. [28]

2.4.1.2 *Hypersonic Cruise Vehicle (HCV)*

HCV describes a generic class of vehicles capable of maintaining hypersonic speeds under thrust for sustained periods of time. At the moment, HCVs are conceptual, but include several projects such as MA3A, DARPA sponsored FALCON, Black-swift, and X-51. The US military is seeking an unmanned HCV capable of delivering 12,000 lbs of payload that can reach any target within a range of 9,000 nautical miles in less than two hours [2, 23].

An extension of this research directly applies to HCVs, specifically the addition of thrust to the equations of motion. The HCV that burns out of thrust is subject to the same dynamics as the CAV.

2.4.1.3 *Reusable Launch Vehicle (RLV)*

The term RLV comes from NASA's Reusable Launch Vehicle program. The program is now into its Second Generation RLV program, and is also known as the Space Launch Initiative. The goals of the program are:

> NASA's Reusable Launch Vehicle (RLV) program has dual objectives: to demonstrate technologies leading to a new generation of space boosters capable of delivering payloads at significantly lower cost, and to provide a technology base for development of advanced commercial launch systems that will make U.S. aerospace manufacturers more competitive in the global market. [5]

An RLV would then only require refueling for subsequent returns to space.

RLVs are considered important beneficiaries of this research. In general, an RLV will either need to fly back to its home designation or maneuver to another facility downrange. The decision to turn around and fly home or continue on to another landing site is contingent upon the time of payload separation and whether the vehicle has enough energy and control authority to make the return trip.

2.4.2   X-15

In 1954 the X-15 became the first suborbital airplane. The X designation denotes the plane as an experimental vehicle, but also, and more importantly as a high altitude research vehicle. It significantly "contributed valuable research information in the supersonic and hypersonic speed regime up to the fringes of space" and expanded our understanding and modeling of the atmosphere [24]. The X-15 is not capable of taking off from the ground on its own; therefore it is attached to a B-52 which will release it midair. Figure 4 shows the X-15 separating from the B-52.

Figure 4. This photo, taken from a B-52, pictures the X-15 immediately after launch with an F-104 flying chase [7].

2.4.3 Dynamic Soarer (Dyna-Soar)

Perhaps the first CAV-like design, the Dyna-Soar, also known as the X-20, was a proposed spaceplane. It was designed to be a multi-purpose vehicle that would be boosted to orbit and then glide to its destination. In addition to orbital bomber and reconnaissance missions, designers also added satellite maintenance and sabotage missions to its list of capabilities. Ultimately the project was cancelled in 1963 due to budget overruns and technical hurdles. Although this project never got off the ground, the research and design concepts made its way into other projects such as the Space Transport System (STS), and many of the planned capabilities are now incorporated in the Air Force's current Global Reach concepts [21].

Figure 5. Boeing's mockup of the X-20 [3].

2.4.4 Space Transport System (STS)

STS, better known as NASA's Space Shuttle, could be considered an RLV and a CAV. The STS includes the orbiter, solid rocket boosters and external fuel storage tank. The solid rocket boosters and external tank are jettisoned after launch, but the boosters parachute down for recovery and reuse (unlike the external tank). Additionally, the Shuttle's return to Earth begins as a hypersonic unpowered glide which is similar in

description to the CAV, but unlike the CAV the Shuttle is not dispensing a cargo or payload while in the atmosphere.

Figure 6. Discovery shuttle and STS 120 crew on launch to the International Space Station [6].

2.4.5   *Flexible Aerospace System Solution for Transformation (FASST)*

"The Boeing FASST concept is a horizontal takeoff, horizontal landing (HTHL), two-stage-to-orbit (TSTO) reusable vehicle with a turbine-based propulsion system on the first stage and a rocket-based combined cycle (RBCC) powered second stage" [10].

FASST is a response to NASA's Integrated Space Transportation Plan/Program (ISTP) which seeks to expand the civil and commercial reach into space for the coming decades. The plan details the development of RLVs for use in delivering cargo to Low Earth Orbit (LEO). The turbine stage of the vehicle is set for an upper limit of Mach 4 [19].

2.4.6   Force Application Launch from Continental United States (FALCON)

FALCON is currently a DARPA sponsored project whose "objectives are to develop and demonstrate hypersonic technologies that will enable prompt global reach missions" [2]. The project expands upon the path of developing a HCV and has already spawned several sub-projects labeled as Hypersonic Technology Vehicle(s) (HTV). This test bed of vehicles will be used to validate affordable and responsive space lift capabilities.

2.5   Closing Remarks

This chapter presented the dynamic optimization problem and briefly discussed techniques used to solve the sensitivity problem. The verification of the optimality of the results obtained from the pseudospectral solver is expounded upon in Maj. Jorris' dissertation [23]. Additionally, several real world vehicles, to which this research may potentially apply, were introduced.

During the course of this research, the software written by Anil Rao, and used herein, changed names from GPOCS to OPENPOCS to GPOP to PSCOL. Each name change signifies either a change in code structure, licensing, or product affiliation, but the software maintained the underlying GPM. In its current release, PSCOL can also do both the LPM and Radau Pseudospectral Method (RPM). This research uses OPENPOCS for legacy reasons, although any pseudospectral method may be considered.

III. Problem Definitions and Assumptions

3.1 Generic Problem Statement

The overall objective of this research is to obtain the optimal trajectory for a given vehicle to reach its target in a minimum amount of time and to study the sensitivity of the terminal state due to variations in waypoint location(s). The optimal solution to the two-point boundary-value problem will serve as the baseline or nominal solution to which comparisons will be made.

Additionally, a verification of the need for a higher fidelity model is sought. Without argument, people accept that the Earth is spherical (the Earth is actually an oblate spheroid), and a flat Earth model is insufficient for any orbit problem including re-entry; therefore, without further consideration, the flat Earth model is rejected in lieu of the spherical Earth model. The verification then rests on the need to include Earth's rotation in the model.

3.2 Mission Assumptions

The assumptions are broken into three classes: mission components, vehicle components, and environmental components. Mission components include target and waypoints. Vehicle components include equations of motion and control limitations.

3.2.1 Mission Components

Similar mission assumptions are taken from [23]:

1. The waypoints are specified in the desired sequence.

2. Waypoint passage must be through a radial originating from the center of the Earth.

3. Altitude for waypoint passage is not specified.

4. Inner-loop control is available. Only the outer-loop or trajectory generation is addressed.

5. Target coordinates and final altitude is specified.

3.2.2 *Vehicle Components*

1. Vehicle is modeled as a point mass.

2. Non-thrusting vehicle.

3. Bank angle is the only control parameter.

4. Coefficients of lift and drag are held constant.

3.2.3 *Environmental Components*

1. Spherical Earth model.

2. The atmosphere is modeled as a simple exponential.

3. Rotation of the Earth is turned 'off' initially.

3.2.3.1 *3-D Non-dimensional Equations of Motion*

In numerical dynamic optimization, it is desirable to scale and/or non-dimensionalize the equations of motion such that all the terms involved are near the same order of magnitude. Vinh and Braces' non-dimensional "universal equations" of motion are problematic because they are not scaled appropriately for dynamic optimization solvers. Instead, the dimensional 3D equations of motion from [20] are scaled and non-dimensionalized. The following are the 3D non-dimensional equations of motion. The derivation of these equations is provided in Appendix A.

$$\frac{dr'}{d\tau} = {}^{R}V' \sin \gamma \tag{3.1}$$

$$\frac{d\,{}^{R}V'}{d\tau} = -\frac{\sin \gamma}{r'^2} + r' \omega_{\oplus}'^2 \cos \phi \left(\cos \phi \sin \gamma - \sin \phi \sin \psi \cos \gamma \right) - D' \tag{3.2}$$

$$\frac{d\theta'}{d\tau} = \left(\frac{{}^{R}V'}{r'}\right)\frac{\cos\gamma\cos\psi}{\cos\phi} \tag{3.3}$$

$$\frac{d\phi'}{d\tau} = \left(\frac{{}^{R}V'}{r'}\right)\cos\gamma\sin\psi \tag{3.4}$$

$$\frac{d\gamma'}{d\tau} = \frac{L'}{{}^{R}V'}\cos\sigma - \frac{\cos\gamma}{r'^{2}\,{}^{R}V'} + \frac{{}^{R}V'}{r'}\cos\gamma + 2\omega'_{\oplus}\cos\phi\cos\psi + \ldots$$
$$\ldots + \frac{r'}{{}^{R}V'}\omega'^{2}_{\oplus}\cos\phi\left(\cos\phi\cos\gamma + \sin\phi\sin\psi\sin\gamma\right) \tag{3.5}$$

$$\frac{d\psi'}{d\tau} = \frac{L'\sin\sigma}{{}^{R}V'\cos\gamma} - \frac{{}^{R}V'}{r'}\cos\gamma\cos\psi\tan\phi + 2\omega'_{\oplus}\left(\sin\psi\cos\phi\tan\gamma - \sin\phi\right)\ldots$$
$$\ldots - \frac{r'\omega'^{2}_{\oplus}}{{}^{R}V'}\frac{\sin\phi\cos\phi\cos\psi}{\cos\gamma} \tag{3.6}$$

where r is the radius from the center of the Earth, ${}^{R}V$ is the relative velocity, θ is the longitude, ϕ is the latitude, γ is the flight-path angle, and ψ is the heading angle. The terms (not already defined) on the right-hand side of the equal sign: L is the force due to lift, D is the force due to drag, and $\omega_{\oplus}$ is the rotation rate of the Earth. The prime denotes the values as non-dimensional.

3.2.4   *Mission Profiles and Case Definitions*

Several mission profiles are considered in which the RV will attempt to fly a minimum time trajectory to the target. The cases are designed to investigate the effect of Earth's rotation on generated trajectories, and the last case examined is an example of how a mission strategist might use this tool to select additional waypoints. Each of the cases share the same initial and final target coordinates, but otherwise exhibit a progression of changes. The first mission profile (case 1) is used to validate the equations and solution technique, and it begins with a scenario in which the rotation of

the Earth is turned 'off.' This scenario is then contrasted against the second mission

profile (case 2) where the rotation is turned 'on.' Although Table 1 and Table 2 show the

two cases with identical initial conditions, in reality the initial conditions are different

due to inertial and relative measurements of the velocity and flight-path angle. The

superscript 'R' in the tables is used to denote a relative value. The third mission profile

(case 3) is an extension of case 2 where an intermediate waypoint has been defined. In

all cases, the optimal trajectory is computed between the initial, intermediate (if

defined), and final target. The computed optimal trajectory defines the baseline

trajectory from which the sensitivity analysis stems. The sensitivity analysis is explained

in Section 3.4. Specific values for each case are presented in Table 1 to Table 3

respectively, with the initial, intermediate (if defined), and final state values defined.

Table 1. Case 1 initial and final conditions.

Initial Conditions	Final Conditions
$r_0 = 6500km$	$r_f = 6456km$
$V_0 = 7.3152 \frac{km}{s}$	$V_f = ND$
$\gamma_0 = -1.5°$	$\gamma_f = ND$
$\psi_0 = 0°$	$\psi_f = ND$
$\theta_0 = -80°$	$\theta_f = 11.32°$
$\phi_0 = 34°$	$\phi_f = 3.52°$
$\sigma_0 = ND$	$\sigma_f = ND$
$\omega_\oplus = 0 \frac{rad}{sec}$, $m = 1000kg$, $S = 80m^2$, ND=not defined	

Table 2. Case 2 initial and final conditions.

Initial Conditions	Final Conditions
$r_0 = 6500 km$	$r_f = 6456 km$
$^R V_0 = 7.3152 \frac{km}{s}$	$^R V_f = ND$
$^R \gamma_0 = -1.5°$	$^R \gamma_f = ND$
$\psi_0 = 0°$	$\psi_f = ND$
$\theta_0 = -80°$	$\theta_f = 11.32°$
$\phi_0 = 34°$	$\phi_f = 3.52°$
$\sigma_0 = ND$	$\sigma_f = ND$
$\omega_\oplus = 7.2722 \times 10^{-5} \frac{rad}{sec}$, $m = 500 kg$, $S = 80 m^2$, ND=not defined	

Table 3. Case 3 initial, intermediate, and final conditions.

Initial Conditions	Intermediate Waypoint	Final Conditions
$r_0 = 6500 km$	$r_1 = ND$	$r_f = 6456 km$
$^R V_0 = 7.3152 \frac{km}{s}$	$^R V_1 = ND$	$^R V_f = ND$
$^R \gamma_0 = -1.5°$	$^R \gamma_1 = ND$	$^R \gamma_f = ND$
$\psi_0 = 0°$	$\psi_1 = ND$	$\psi_f = ND$
$\theta_0 = -80°$	$\theta_1 = -22.07°$	$\theta_f = 11.32°$
$\phi_0 = 34°$	$\phi_1 = 21.59°$	$\phi_f = 3.52°$
$\sigma_0 = ND$	$\sigma_1 = ND$	$\sigma_f = ND$
$\omega_\oplus = 7.2722 \times 10^{-5} \frac{rad}{sec}$, $m = 500 kg$, $S = 80 m^2$, ND=not defined		

3.2.5   Vehicle Characteristics

The vehicle characteristics chosen are not specific to any real world vehicle, such as presented in Chapter II. Instead they represent "ballpark" figures that describe a small-to-medium size vehicle (case 1), and a similar size vehicle with half the weight (cases 2 and 3). Since the initial state vector is held constant, a difference in initial kinetic energy is introduced when the rotation of the Earth is turned on. The vehicle weight is

cut in half to reduce the initial inertial kinetic energy and prevent the vehicle from bouncing off the Earth's atmosphere when the rotation of the Earth is turned 'on.' The vehicle characteristics are simply described by the following parameters:

$S = 80m^2$ - wetted surface area

$m = 1000kg$ $(500kg)$ - mass of RV

$C_L = 2$ - coefficient of lift

$C_D = 1$ - coefficient of drag

The vehicle lift and drag coefficients are simplified to be constants. This corresponds to setting the angle-of-attack to a constant, since the lift and drag are primarily a function of angle-of-attack. This is consistent with the defined equations of motion in Section 3.2.3.1 which only include bank-angle as a control. The RV is given a minimum and maximum allowable bank-angle. Such limitations are common on vehicles that are shielded more heavily on one side. Additionally the bank-angle rate is constrained reflecting that the vehicle cannot instantaneously change its bank-angle.

$$
\begin{aligned}
\sigma_{min} &= -60° \\
\sigma_{max} &= 60° \\
\dot{\sigma}_{min} &= -60°/sec \\
\dot{\sigma}_{max} &= 60°/sec
\end{aligned}
\tag{3.7}
$$

3.3 *Optimal Control Problem*

As stated earlier, the objective is to minimize the time of flight; therefore, the dynamic optimization problem is:

Minimize

$$
J = \tau_f \tag{3.8}
$$

subject to the non-dimensional equations of motion, (3.1)-(3.6) as well as the dynamics, representing the relationship between the bank-angle rate and the control input $u(\tau)$.

$$\frac{d\sigma}{d\tau} = u(\tau) \tag{3.9}$$

Adding the bank-angle rate, (3.7), as a state allows for limits on how fast the vehicle can roll. The TPBVP is subject to the event constraints or boundary conditions, specifically: initial altitude, velocity, longitude, latitude, flight-path-angle, and heading, as well as final altitude, longitude, and latitude. These are given as:

$$\phi\big(x(\tau_0),\tau_0,x(\tau_f),\tau_f\big) = \begin{bmatrix} r'(\tau_0)-r_0' \\ {}^R V'(\tau_0)-V_0 \\ \theta'(\tau_0)-\theta_0 \\ \phi'(\tau_0)-\phi_0 \\ \gamma'(\tau_0)-\gamma_0 \\ \psi'(\tau_0)-\psi_0 \\ r'(\tau_f)-r_f' \\ \theta'(\tau_f)-\theta_f \\ \phi'(\tau_f)-\phi_f \end{bmatrix} = 0 \tag{3.10}$$

Additionally, the problem is subject to the inequality constraints on the state (bank-angle) and control (bank-angle rate).

$$C\big(x(\tau),u(\tau),\tau\big) = \begin{bmatrix} \sigma_{min}-\sigma(\tau) \\ \sigma(\tau)-\sigma_{max} \\ \dot{\sigma}_{min}-u(\tau) \\ u(\tau)-\dot{\sigma}_{max} \end{bmatrix} \leq 0 \tag{3.11}$$

3.4 Methodology

This section describes the systematic selection of waypoints used to map the sensitivity of the terminal state. Preliminary experimentation and testing helped define

the flowchart in Figure 7. First, a single phase optimal trajectory is generated using

(3.10) and (3.11) but without any interior point constraints (waypoints). This trajectory

serves as a baseline or nominal trajectory for future computations. Using Bellman's

principle of optimality, the single phase solution is divided into a two-phase solution.

The connection point of the two phases is a waypoint, or fixed latitude and longitude the

RV must pass through. Splitting the trajectory into two phases now provides a

mechanism to precisely define and relocate waypoints. The flow chart outlines the

progression or variation of the intermediate waypoints in a systematic fashion.

The flow chart shown begins with user supplied initial and final conditions.

Specifically altitude, latitude, and longitude are needed for both initial and final

conditions, and in addition to the previously mentioned states, velocity, flight-path

angle, and heading angle are required for the initial condition. The remaining sequence

of events is hands-off for the user. The continuous time problem is discretized and

evaluated at n LG nodes to solve the baseline optimal trajectory from the initial to final

target. Each node of the baseline optimal solution then becomes a waypoint, and at this

point the single phase trajectory is divided into many two-phase trajectories. New

optimal control problems are created by incrementally shifting the waypoint north by

'dphi' degrees. The optimal trajectory is found through each new waypoint position,

and the process of incrementing by 'dphi' continues until a solution cannot be found.

'dphi' was chosen to be a relatively small value, i.e. 'dphi' $= 0.01°$ (~0.6 nmi), to aid in the

convergence rate of the GPM solver which uses the nearest computed trajectory as an

initial guess for the new waypoint. Larger values of 'dphi' may be used, but it increases

the likelihood the GPM solver will not converge since the initial guess is comparatively
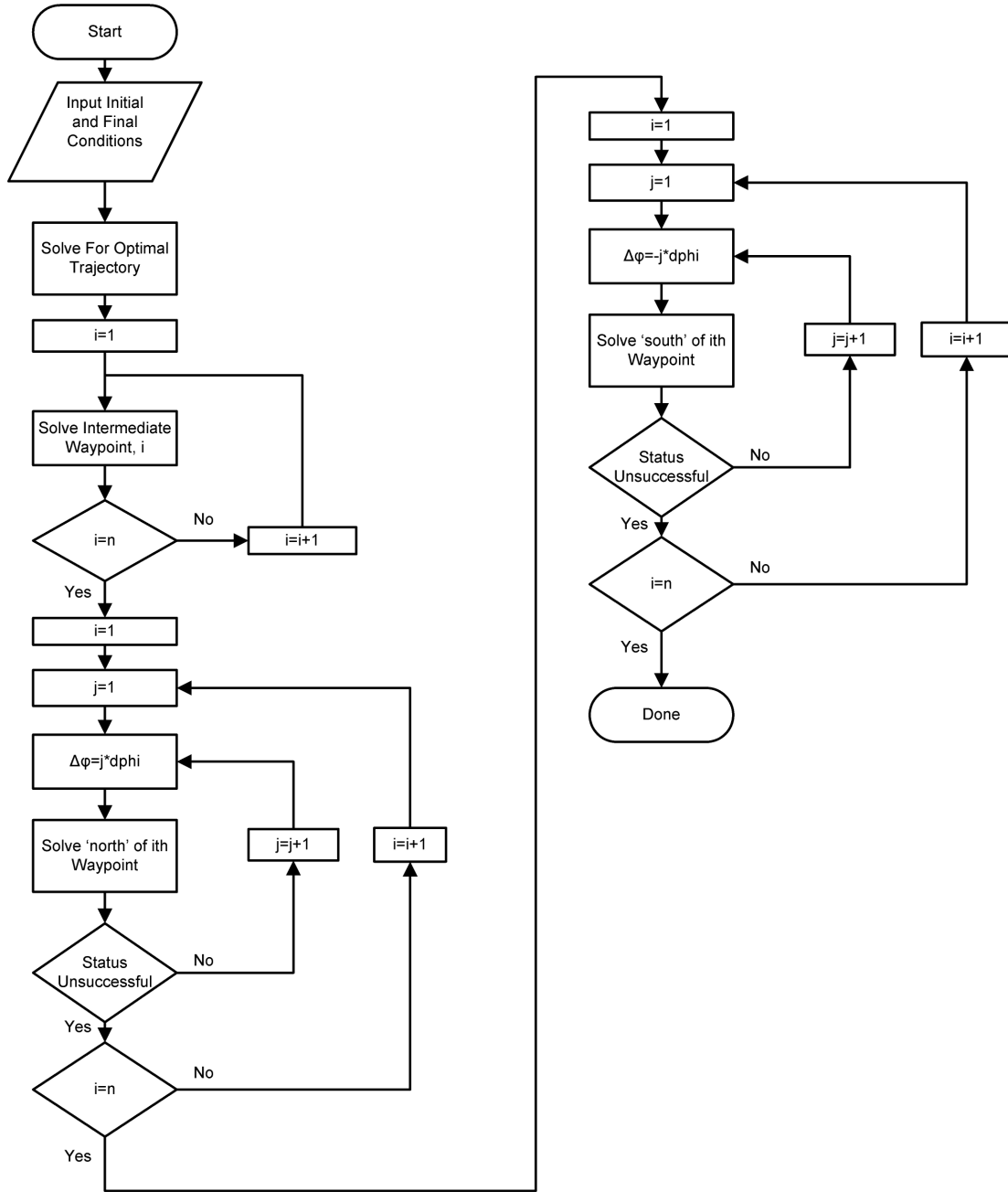
Figure 7. Basic algorithm used to map sensitivity.

farther from the optimal solution. The exact specifics of what constitutes an

unobtainable solution will be explained later. Next, the same procedure is repeated,

incrementally shifting the waypoints south. Note that the solution is optimal at the nodes and it is assumed that the solution is near optimal elsewhere. Splines are used to interpolate between the nodes and provide a more accurate solution. Tabulating the terminal state values associated with each waypoint then describes how the terminal state changes with waypoint location, providing the desired 'mission objective' sensitivity to the waypoint.

Figure 8 visually conceptualizes the process in the flowchart. First, the baseline optimal solution between the initial and final target is computed shown by the solid line. Then, starting from a location on the baseline optimal trajectory, waypoints are incrementally stepped along a longitude in both directions in a uniform increment. At each new waypoint, the optimal trajectory through the new waypoint is calculated shown in dashed lines. Once a trajectory is considered unobtainable, the process would then repeat by starting over at a new location along the baseline trajectory.

There are several automated 'stop' conditions in the software code that are used to manage the iteration control and convergence criteria the program uses to obtain a solution. A 'stop' condition is a message to the program to stop stepping the waypoint north or south, and move on to the next waypoint location on the baseline solution. Since this research is primarily interested in the immediate surrounding area of the baseline solution, there is a limit on the number of incremental steps a waypoint may be moved north or south. A 'stop' condition may also be triggered if the underlying optimization solver returns back status codes corresponding to infeasible solutions or other unexpected termination status codes. Before the 'stop' condition is triggered, the program increases the number of nodes in each phase and attempts to re-solve the

problem. Once the number of nodes in each phase has reached a limit, then the 'stop'

condition is triggered. The justification for increasing the nodes is presented in Section
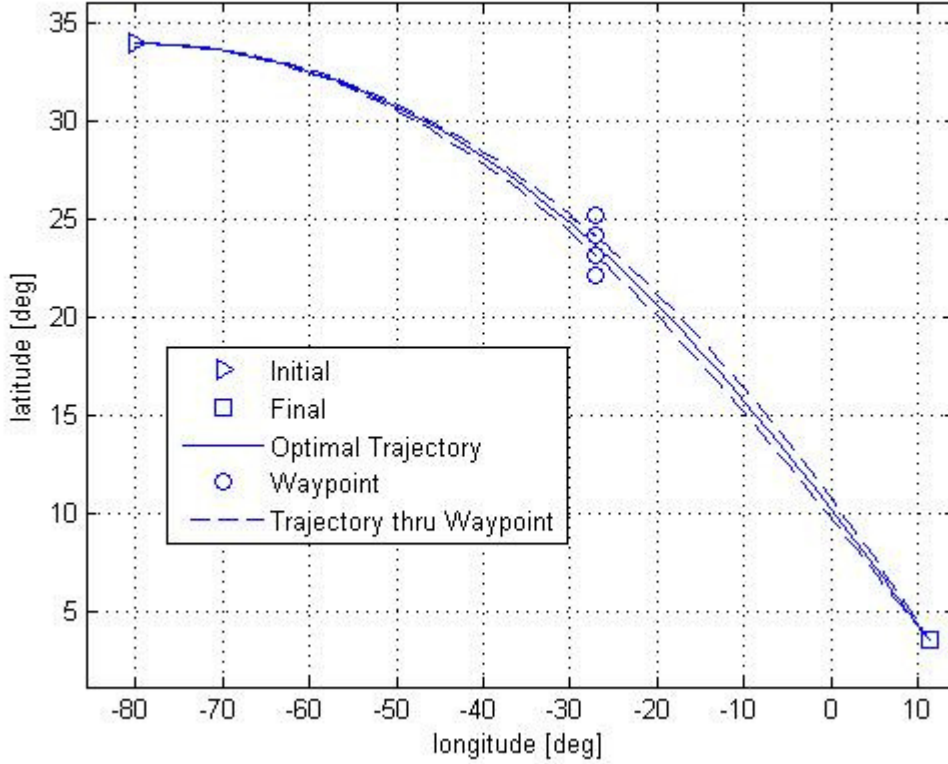
4.1.

Figure 8. Waypoint selection process w.r.t. optimal trajectory.

This methodology meets the objectives of the research by solving the baseline

optimal control problem, and then sampling the neighboring area for fixed waypoints

and re-solving the optimal trajectory to obtain sensitivity data. The expected results are

a range of feasible solutions that fall in an envelope surrounding the baseline trajectory.

Specifically, the time-to-target will increase, and the terminal velocity will decrease as

the RV maneuvers to waypoints farther off the baseline trajectory. The results obtained

using this approach is discussed in Chapter IV.

IV.   Analysis and Results

In this chapter, the analyses of the three cases defined in Chapter III are used to present a unifying trend among all re-entry trajectories. Specifically, cases 1 and 2 are similar in problem setup and vehicle dynamics, but they differ in vehicle mass and Earth rotation rate. The last case is more of a demonstration of the further capabilities of this solution technique. The numerical result obtained from each of the cases fulfills the objective of identifying the sensitivity of the terminal state to variations in waypoint location.

4.1   Node Analysis

The amount of time to compute an optimal solution in general increases as more nodes are used in the solution. Recall a node represents a discrete time in the continuous time dynamics. The added benefit of using more nodes is obtaining a more accurate solution; therefore, the motivation for this portion of the analysis is to identify a minimum number of nodes that should be used in calculating solutions, balancing computing time and ensuring accuracy in the solution.

To establish a true baseline, an initial state vector was chosen and integrated forward for approximately 2000 seconds using MATLAB's ode45 integrator. The control variable (bank-angle) was fixed at $0°$ for the entire trajectory. Now using the altitude, latitude, and longitude at 2000 seconds as the final target vector, the initial and final vector are fed into the pseudospectral solver for processing. The state vector and vehicle parameters supplied to the program are listed in Table 4.

Despite the pseudospectral solver returning successful messages of convergence to an optimal solution, the pseudospectral solver generated differing trajectories based

on the number of nodes used. Fortunately, the results increased in accuracy as the number of nodes increased, i.e. more closely matched the baseline. To elucidate, solutions for twenty-one nodes and sixty-one nodes are investigated.

Table 5 shows the resultant terminal state vector obtained from using an ode45 solver, and a pseudospectral solver with twenty-one and sixty-one nodes respectively. Notably the twenty-one node solution differed significantly from the baseline (ode45) in both terminal state conditions and the amount of time required to reach the target. In contrast, the sixty-one node solution nearly matched the true solution with exception to the final bank angle.

Figure 9 shows the altitude of the respective solutions with respect to time. A cubic polynomial is fit through the nodes, represented by 'x's. Note, the blue and green lines corresponding to the sixty-one node and ode45 solutions are indistinguishable from each other. Graphically it is quite apparent that using twenty-one nodes will not suffice. Towards the middle of the trajectory where the nodes are spread the farthest, the solution using twenty-one nodes is unable to capture the true dynamics. This is a consequence of the sampling rate and is remedied by increasing the sampling rate or increasing the number of nodes used.

Table 4. Initial and final state vectors supplied to the optimal solver.

Initial Conditions	Final Conditions
$r_0 = 6500 km$	$r_f = 6456 km$
$V_0 = 7.3152 \frac{km}{s}$	$V_f = ND$
$\gamma_0 = -1.5°$	$\gamma_f = ND$
$\psi_0 = 0°$	$\psi_f = ND$
$\theta_0 = -80°$	$\theta_f = 11.32°$
$\phi_0 = 34°$	$\phi_f = 3.52°$
$\sigma_0 = ND$	$\sigma_f = ND$
$\omega_\oplus = 7.277 \times 10^{-5} \frac{rad}{sec}$, ND=not defined	

Table 5. Three terminal state vectors are shown that are propagated from the same initial state vector (see **Table 4**) using MATLAB's ode45 and a pseudospectral solver with 21 and 61 nodes respectively.

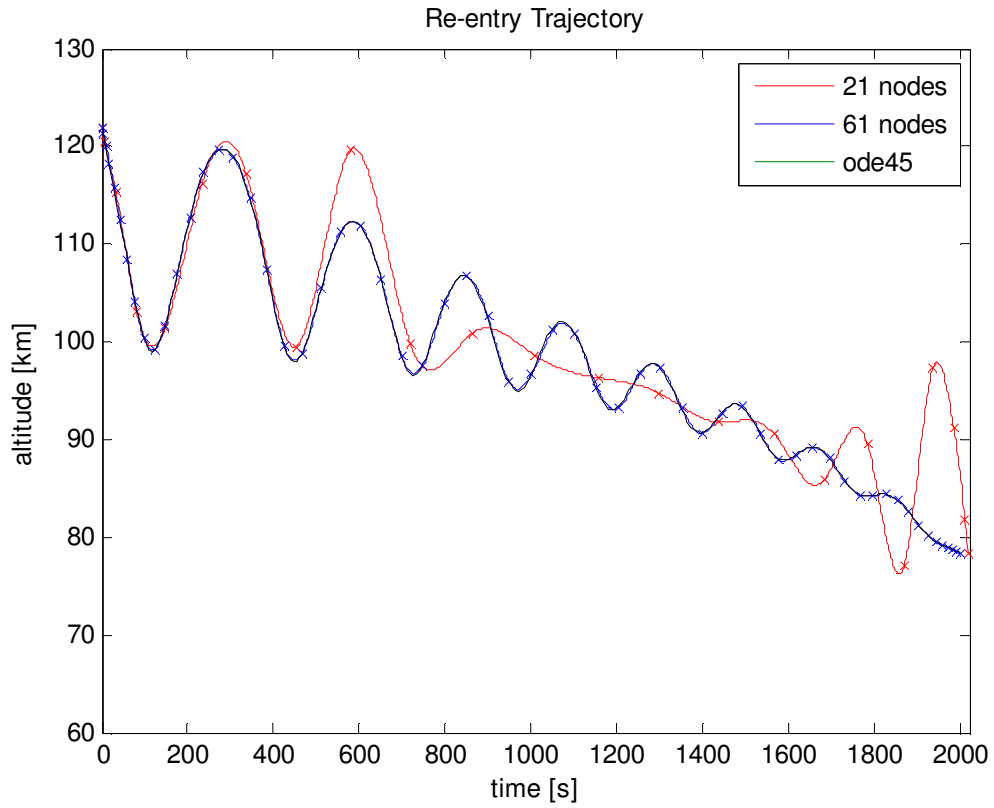|	MATLAB's ode45	21 Nodes	61 Nodes
Final Conditions	$r_f = 6456 km$	$r_f = 6456 km$	$r_f = 6456 km$
	$V_f = 1.592$	$V_f = 1.702$	$V_f = 1.592$
	$\gamma_f = -1.04°$	$\gamma_f = -17.32°$	$\gamma_f = -1.02°$
	$\psi_f = -31.04°$	$\psi_f = -28.51°$	$\psi_f = -31.17°$
	$\theta_f = 11.32°$	$\theta_f = 11.32°$	$\theta_f = 11.32°$
	$\phi_f = 3.52°$	$\phi_f = 3.52°$	$\phi_f = 3.52°$
	$\sigma_f = 0°$	$\sigma_f = 60°$	$\sigma_f = 19.86°$
Final Time	2001 seconds	2016 seconds	2001 seconds

Figure 9. A re-entry trajectory solution generated using 21/61 nodes in OPENPOCS, and a Runge-Kutta 4-5 integrator.
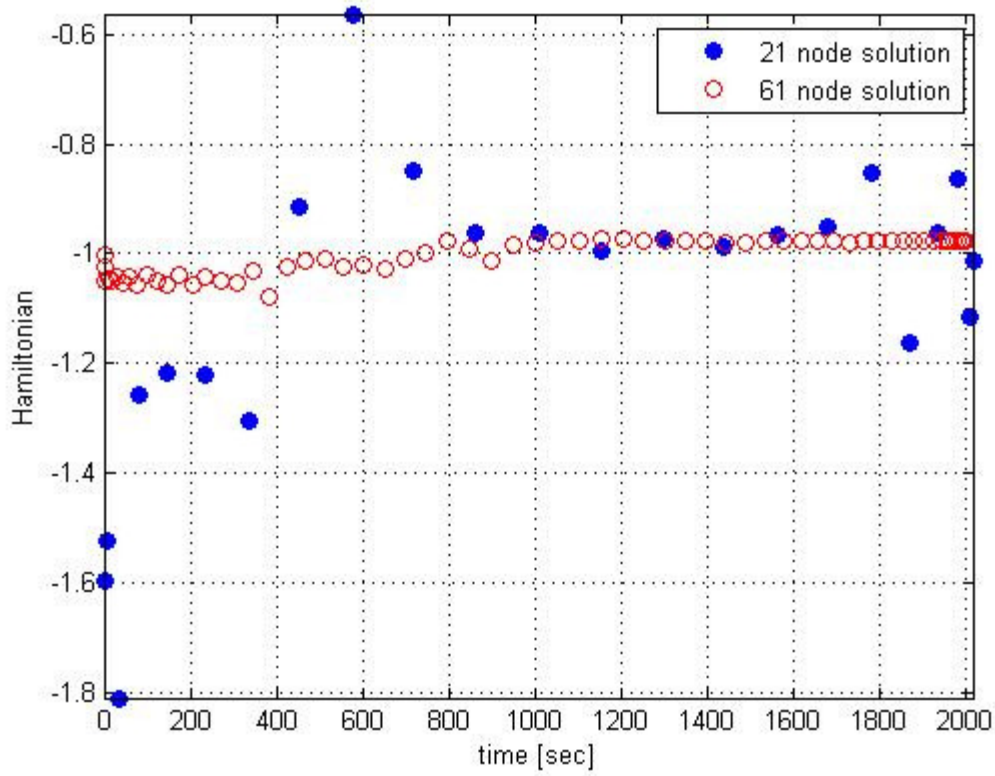
Figure 10. Hamiltonian of 21 and 61 node solutions.

Further, Figure 10 shows the Hamiltonian for each of the solutions. Stated earlier the Hamiltonian of the true optimal solution is equal to a constant, $H = -1$. Clearly the twenty-one node solution is not optimal, and the sixty-one node solution is nearly optimal. Although finding an optimal minimum number of nodes for all trajectories is beyond the scope of this research, it is clear that more nodes are better. For the sensitivity study herein, the sixty-one node solution will be considered adequate; therefore, for further calculations, a minimum of sixty-one nodes is used for the global solution.

4.2   *Rotation Effects*

The inclusion of the rotation rate of the Earth is a significant parameter in modeling reality. Figure 11 shows the range of a re-entry vehicle in constant zero-degree bank-angle flight independent of initial heading angle for the Earth rotation both 'off' and 'on.' Note that the figure shown is a flat representation of the spherical Earth, e.g. a Mercator map projection. To ensure a true comparison, the inertial velocity (kinetic energy) and flight-path angle of the RV are held constant. With the rotation of the Earth 'off', the RV reaches targets in all directions at an equal distance and reaches the ground at the same time regardless of heading. For the rotating Earth, the relative velocity and flight-path angle will vary as the heading angle changes. Consequently, the solid line, depicting Earth's rotation 'on', shows that the RV travels farther in a westerly direction and shorter in an easterly direction. Note that the RV will also reach the ground at different times. The footprint is not merely shifted to the west, but it is also slightly skewed due to the fact that the Earth below the RV moves at a different rate as a function of latitude. It should be noted that the impact footprint size is a function of the vehicle's lift-to-drag ratio (L/D). This is because L/D is a measure of aerodynamic efficiency, and in general, aerodynamic efficiency and range are roughly directly proportional. Thus, Figure 11 is only applicable for the vehicle defined in Table 2, and would need to be recomputed for other vehicle configurations. In conclusion, final targets that were obtainable with the stationary Earth model may now be infeasible with the rotation turned 'on.'

Figure 11 was created by choosing an initial inertial state vector, and then propagating the state forward in time until the RV hit the ground (altitude equals zero).

For the rotating Earth, the initial inertial velocity and flight-path angle are preserved by transforming the state vector from Earth Centered Inertial to the Earth Centered Earth Fixed reference frame as defined in Appendix C.
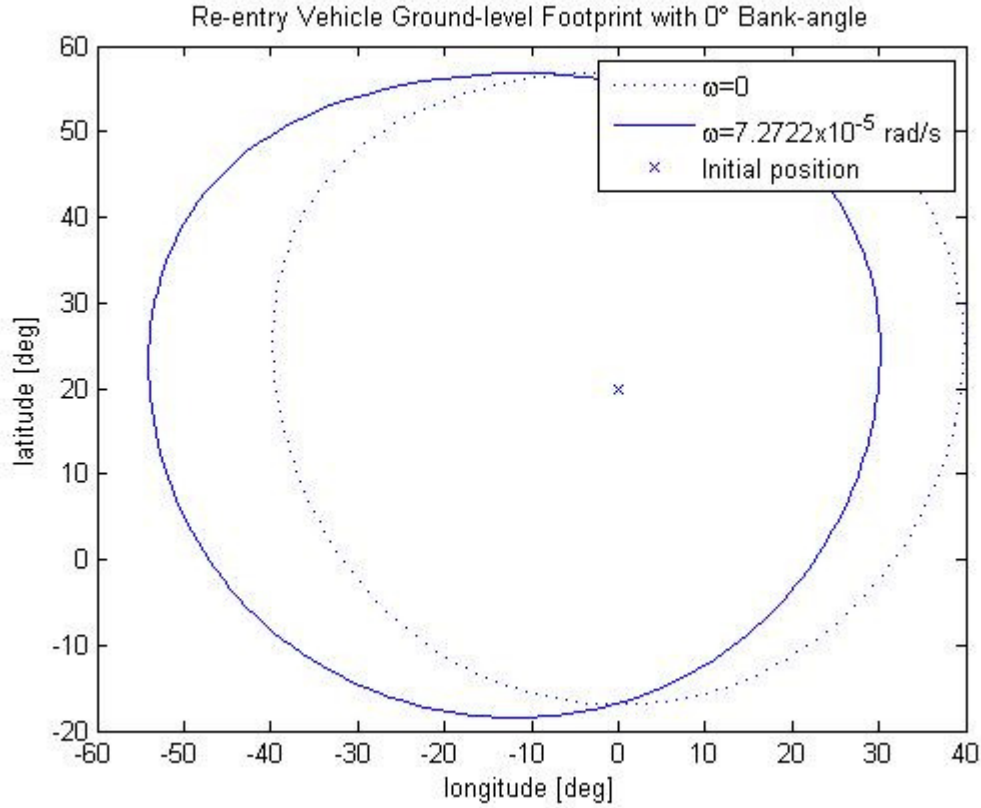

Figure 11. Range of a re-entry vehicle with and without the rotation of the Earth included in the dynamics.

4.3   Case 1 Results and Analysis

The optimal solution to the TPBVP with constraints is solved using the GPM. An initial "point-to-target" guess is provided to the solver by integrating the initial conditions forward for 2000 seconds. To simplify the integration, the bank-angle is fixed to zero degrees.   This choice of initial guess is simply an engineering judgment. Integrating the initial conditions is a means of providing a state history that satisfies the

equations of motion, and 2000 seconds (~33 min) is a reasonable estimate of the flight duration.

The solution obtained from the first iteration of the GPM solver has a low number of nodes (Recall, it is easier to obtain an initial solution with a small number of nodes compared to a large number of nodes), and as discussed earlier, this solution is not optimal. The solution obtained, however, is used as the estimate for the next iteration. At each iteration the number of nodes is incrementally increased until the minimum of sixty-one nodes is reached. Figure 12 shows the states for the optimal solution with sixty-two nodes. In the last subplot showing the bank angle, the RV appears to perform a rapid bang-bang maneuver in bank angle towards the end of the trajectory. Investigation into this behavior shows that this maneuver is much smoother than it appears (see Section 4.6), and results in what is called an 'S' turn, named after the apparent path of the vehicle as viewed from overhead. This last minute 'S' turn allows the RV to change its flight-path angle and perform a dive to the target altitude. The fifth subplot confirms that the flight-path angle has steepened, reaching nearly $-3°$. Additionally, the dive signifies that the RV is dumping energy in order to reach the target altitude, but, if needed, has excess energy available to maneuver to additional waypoints. The use of this excess energy to reach additional waypoints is precisely the motivation behind this research.
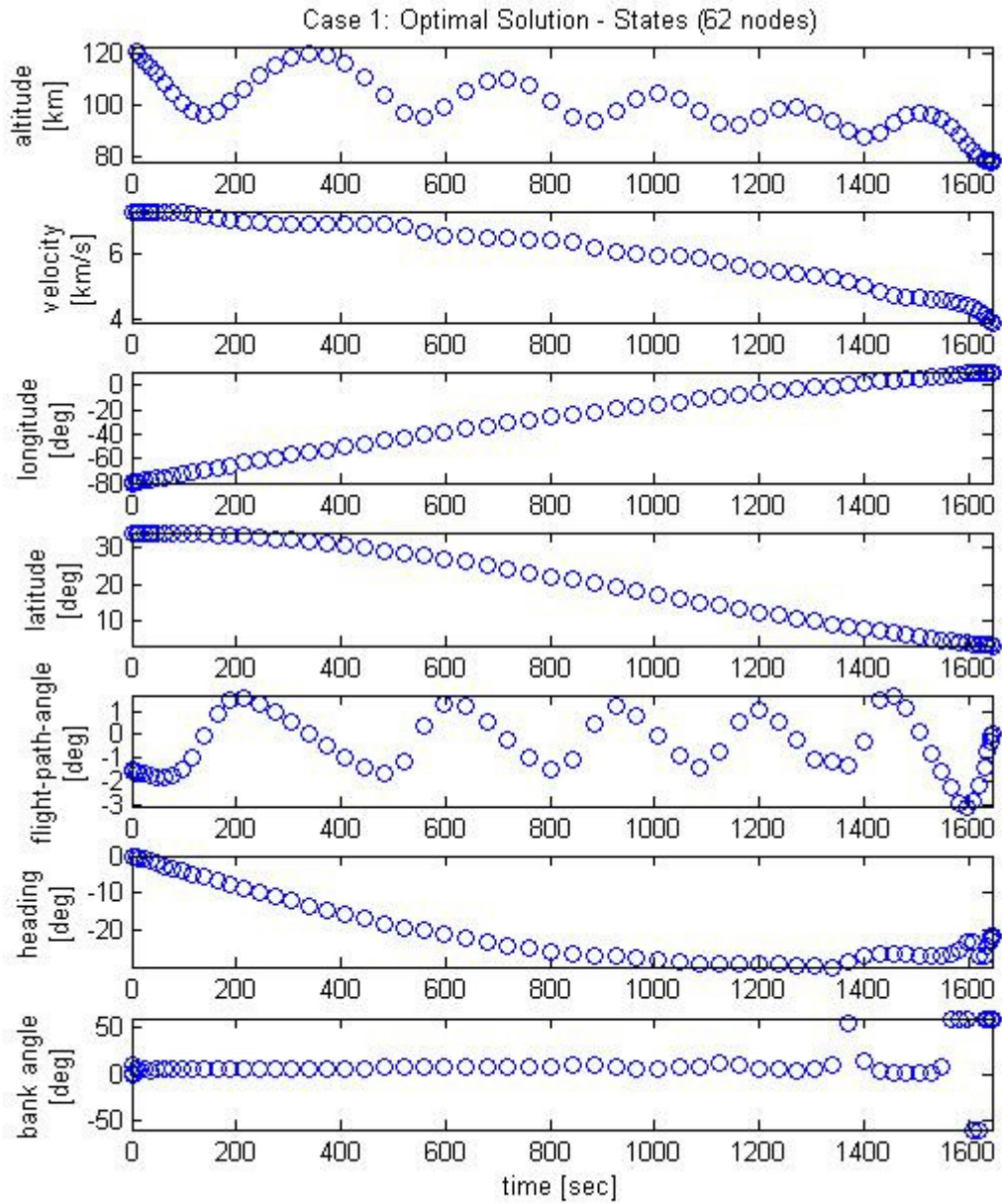
Figure 12. Case 1 results for the optimal solution without predefined waypoints.

Once the baseline solution is computed, the program goes about the task of

systematically moving the waypoints and re-computing a solution. The GPM solver

automatically interpolates the guess to fit the new node locations using cubic

43

interpolation. Occasionally the interpolated guess results in exaggerated states (similar to the Runge phenomenon), and the GPM solver is unable to converge to a solution. One method, which has been semi-successful, is to select another set of nodes to interpolate. This is accomplished in the code by incrementing the number of nodes used in the solution. Consequently an upper node limit is defined so that the algorithm does not continue indefinitely if the GPM solver is continually unsuccessful. It is also expected that as the waypoints are pushed further away from the nominal trajectory, an infeasible solution will be encountered. An infeasible solution is one in which the RV does not have enough energy or maneuverability to both reach the waypoint(s) and final target. Thus, the upper node limit also serves to define a boundary between feasible and infeasible solutions.

The next part of the algorithm, as shown in Figure 7, splits the optimal solution into two phases adjoined at the latitude and longitude corresponding to the interior nodes of the optimal solution. The connection of the two phases at a defined latitude and longitude defines a waypoint. Potentially there are sixty-two two-phase combinations; however, the first 15% and last 15% of the nodes from the optimal solution are not evaluated under the assumption that the variation will be small and are of less interest to the mission planner. Later evidence shows that this assumption is partially true, since the RV is still capable of making 'large' maneuvers near the end of the trajectory; in which case, the last 15% of nodes should not be omitted. For this study, of the original sixty-two nodes, only the interior forty-four nodes are considered. Each of the two-phase combinations is then re-solved for the optimal solution. A conclusion from Bellman's principle of optimality translated to this current problem states that

44

starting at any point on the optimal trajectory results in the new optimal trajectory following the same optimal trajectory [8]. As a result, there are ideally forty-four identical trajectories.

The algorithm then moves the waypoints north and south in increments of $0.01°$ (~0.6 nmi) and re-solves the optimal control problem. The results from progressively moving the waypoints away from the nominal solution are presented in Figure 13. The right facing triangle is the RV starting position, and the dashed line is the optimal trajectory without defined waypoints. The upright and upside-down triangles mark both the longitudinal meridian that the waypoint is pushed along and the sampling bounds. For case 1, an iteration limit of 100 is imposed, and therefore, the total angular difference between the two triangles is $2°$ (~120 nmi). Stated earlier, the algorithm continues to push away from the nominal trajectory until an upper node limit is reached or until the algorithm reaches an iteration limit. This termination decision results in two prominent features as shown in Figure 13. There is a smooth expansion region followed by a straight leg and finally a 'chunk' of data missing. The smooth expansion is indicative of a boundary between feasible and infeasible solutions, whereas the straight leg section is where the algorithm reached the iteration limit. The figure also shows a 'chunk' of missing data that is thought to be an anomaly created by the algorithm terminating too soon. It is also noted that the contour information provided is limited to the region of waypoint sampling. This last comment will become more apparent later in case 3.
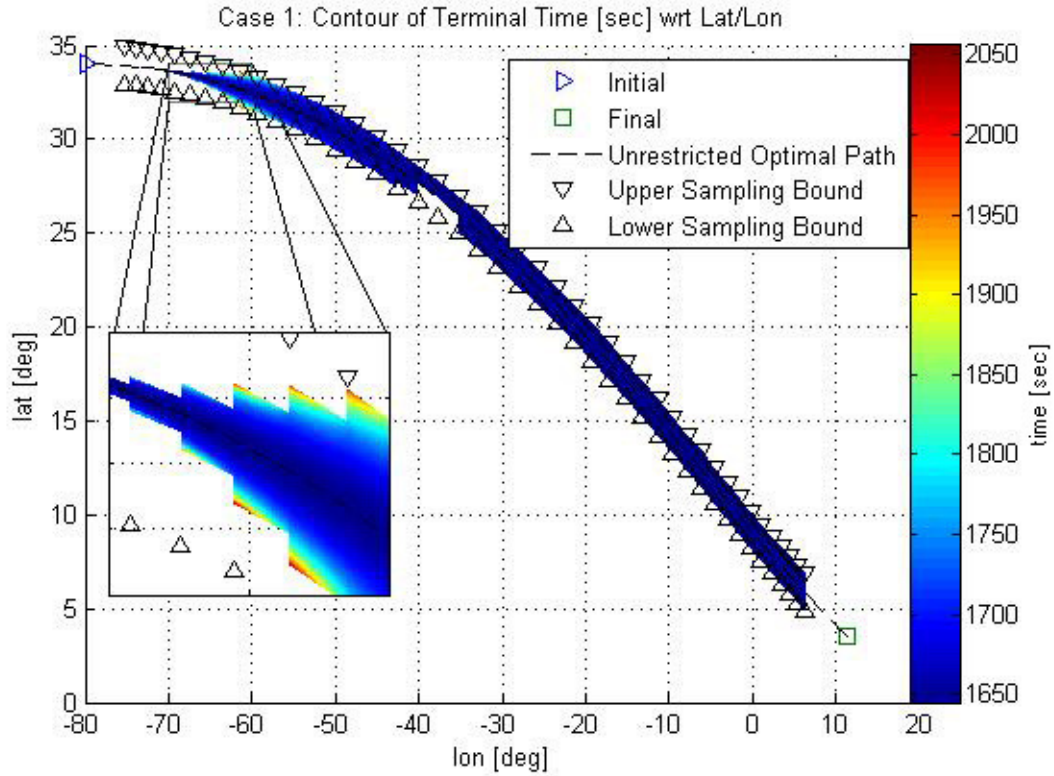
Figure 13. Case 1 contour of terminal time w.r.t. Lat/Lon.

Figure 13 shows the cost of the dynamic optimization problem for each waypoint. As waypoints are chosen off the baseline optimal trajectory, the cost (time to the final target) increases. Further, the terminal time is more sensitive to waypoint location early on in the trajectory as opposed to later in the trajectory. This figure does not adequately capture the contour behavior towards the end of the trajectory, but closer analysis shows the cost does become more sensitive to waypoint selection near the end of the trajectory.
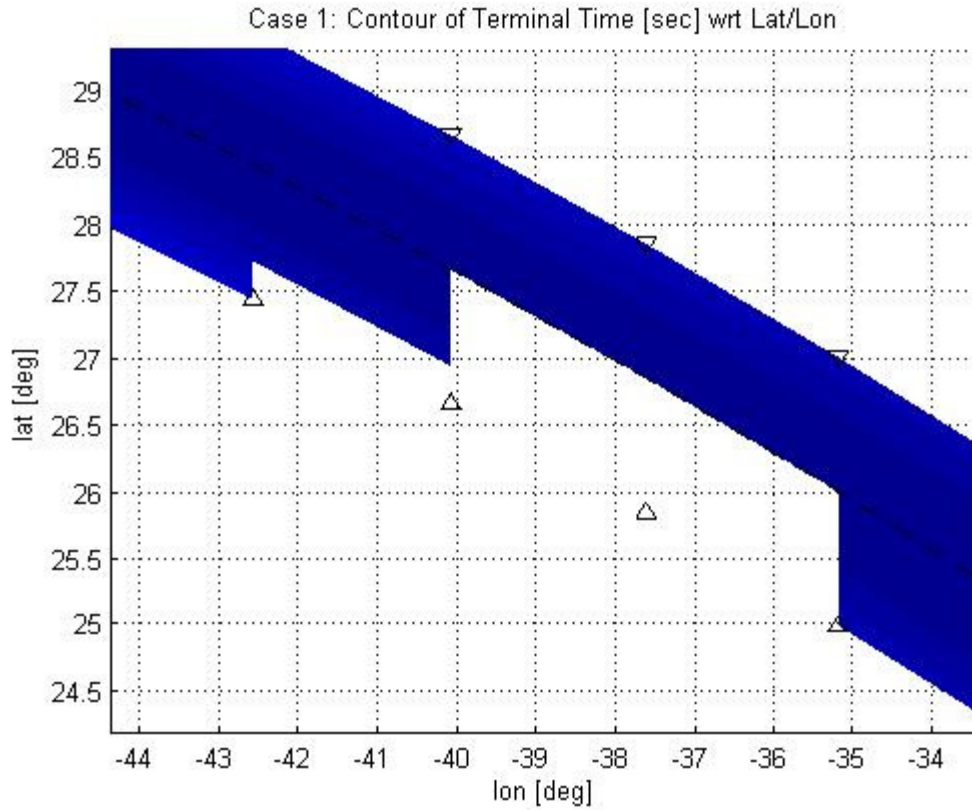
Figure 14. Magnification of Figure 133 highlighting 'missing' piece.

Figure 14 identifies two locations that the algorithm prematurely triggered a 'stop' condition as defined in Section 3.4. This is a fact verified by plotting the trajectories from the neighboring slices and observing their passage through the empty region. This result is a byproduct of automating the process and does not account for every exit scenario. It is wholly possible to go back into the code and tweak the step-size or other parameters until a solution is found, but the exact reason why the program terminated prematurely is lost in the automation process. Ensuring a solution when using an automated process is a topic for future research.

Figure 15 exhibits the same features as Figure 13 except that the velocity

decreases as waypoints are chosen away from the unrestricted optimal solution.
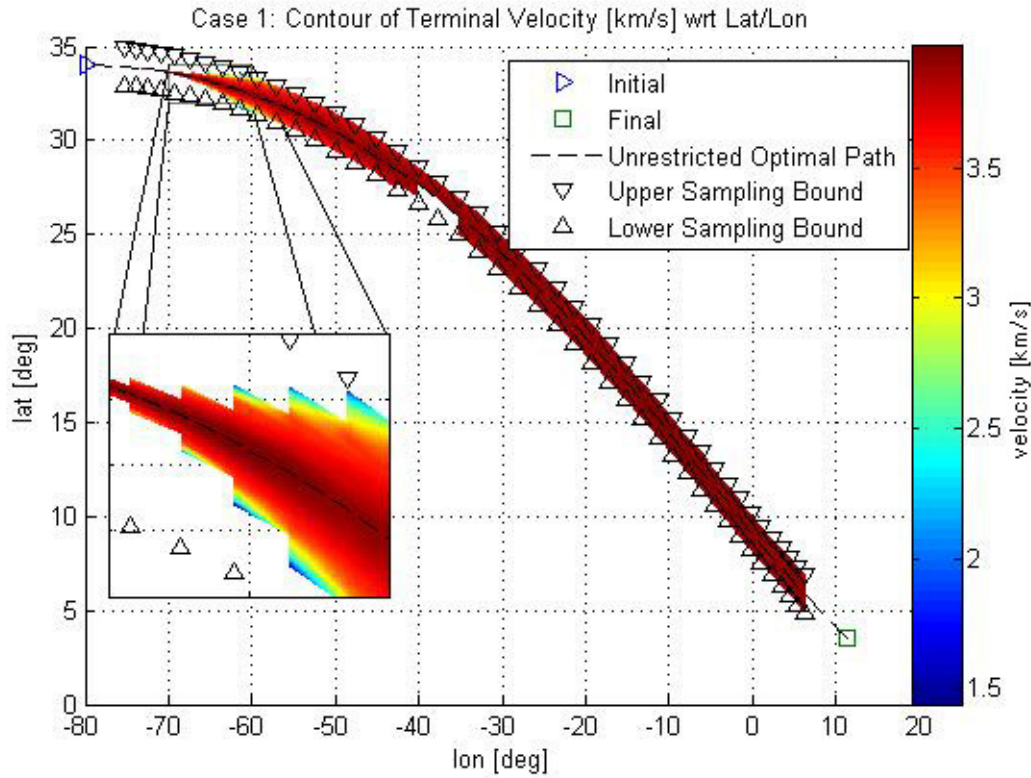
Figure 15. Case 1 contour of terminal velocity w.r.t. Lat/Lon.

In between each vertical triangle pair exists optimal trajectories that pass through

neighboring latitudes at the same longitude. Waypoints that share the same longitude

are a family of waypoints that make up a slice of the region of feasible waypoints

(meridian slices). By plotting the family of waypoints we can visualize the sensitivity of

the optimal trajectory at distinct longitudinal locations. Figure 16 to Figure 18 show the

terminal states of three such families of waypoints. In each figure, only the terminal

time and velocity appear to carry the same parabolic shape from one family of

waypoints to another. The physical interpretation and potential significance of the

discontinuous breaks in the flight-path angle and bank angle are not yet understood, but the results are provided.
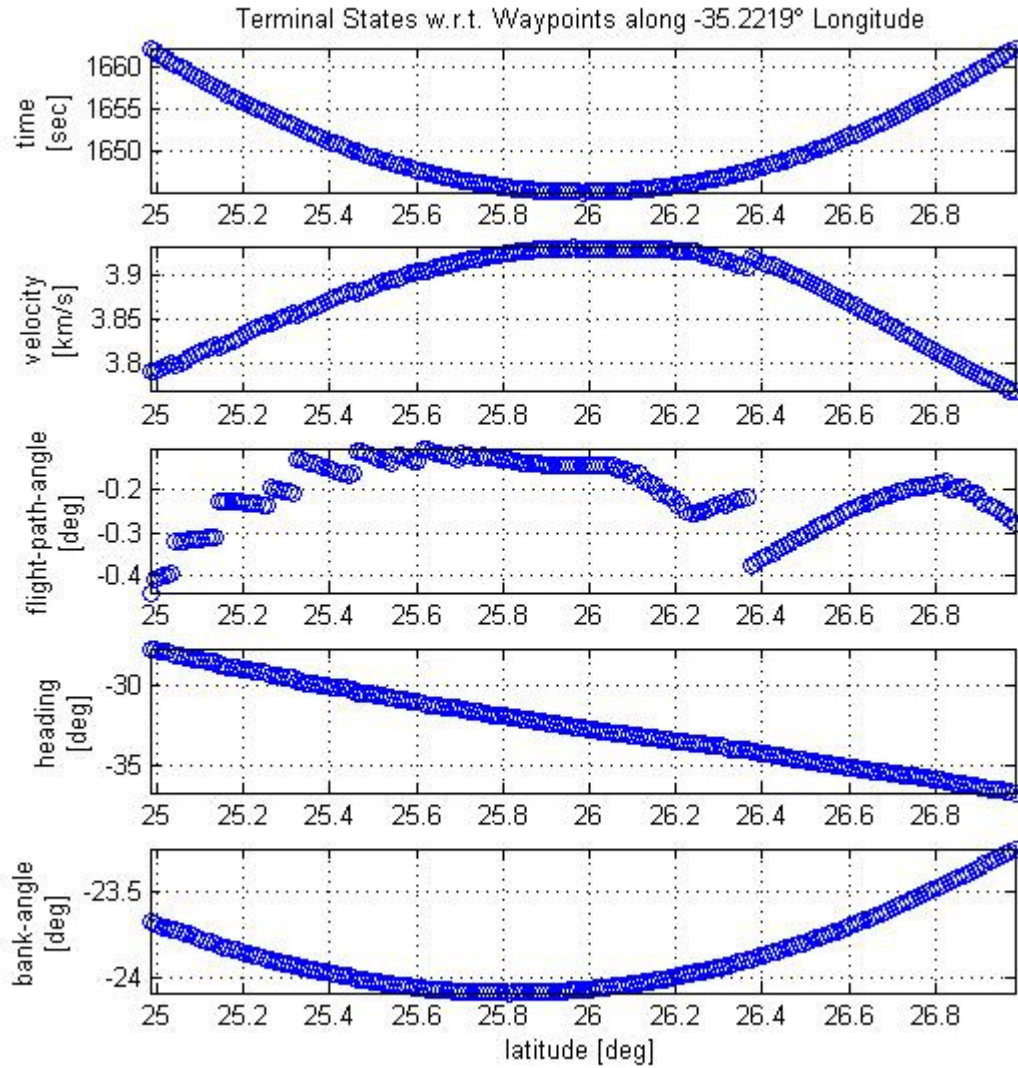

Figure 16. Case 1 terminal states with waypoints along longitude $-35.2219°E$

At approximately $26.4°$ latitude, the RV has a slight bump up in velocity which appears to directly correspond to the steeper flight-path angle. Logically this makes sense; the steeper flight-path angle allows the RV to fall faster to the Earth, and therefore

it picks up additional speed. Note also, the heading angle appears to change nearly

linearly with waypoint location.
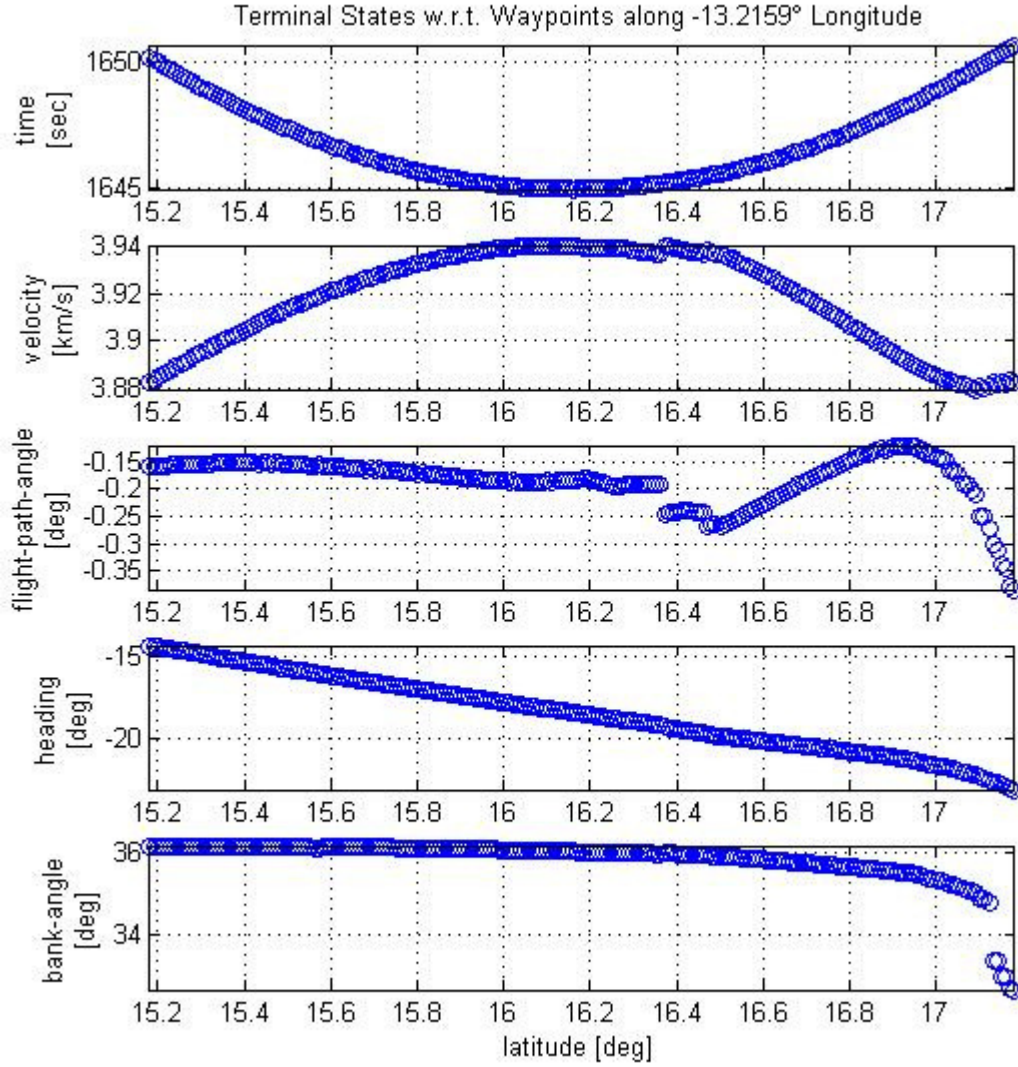
Figure 17. Case 1 terminal states with waypoints along longitude $-13.2159°E$

The increase in velocity seen towards the latter portion of the trajectory (right

end) is associated with the RV performing a last minute dive to the target altitude.
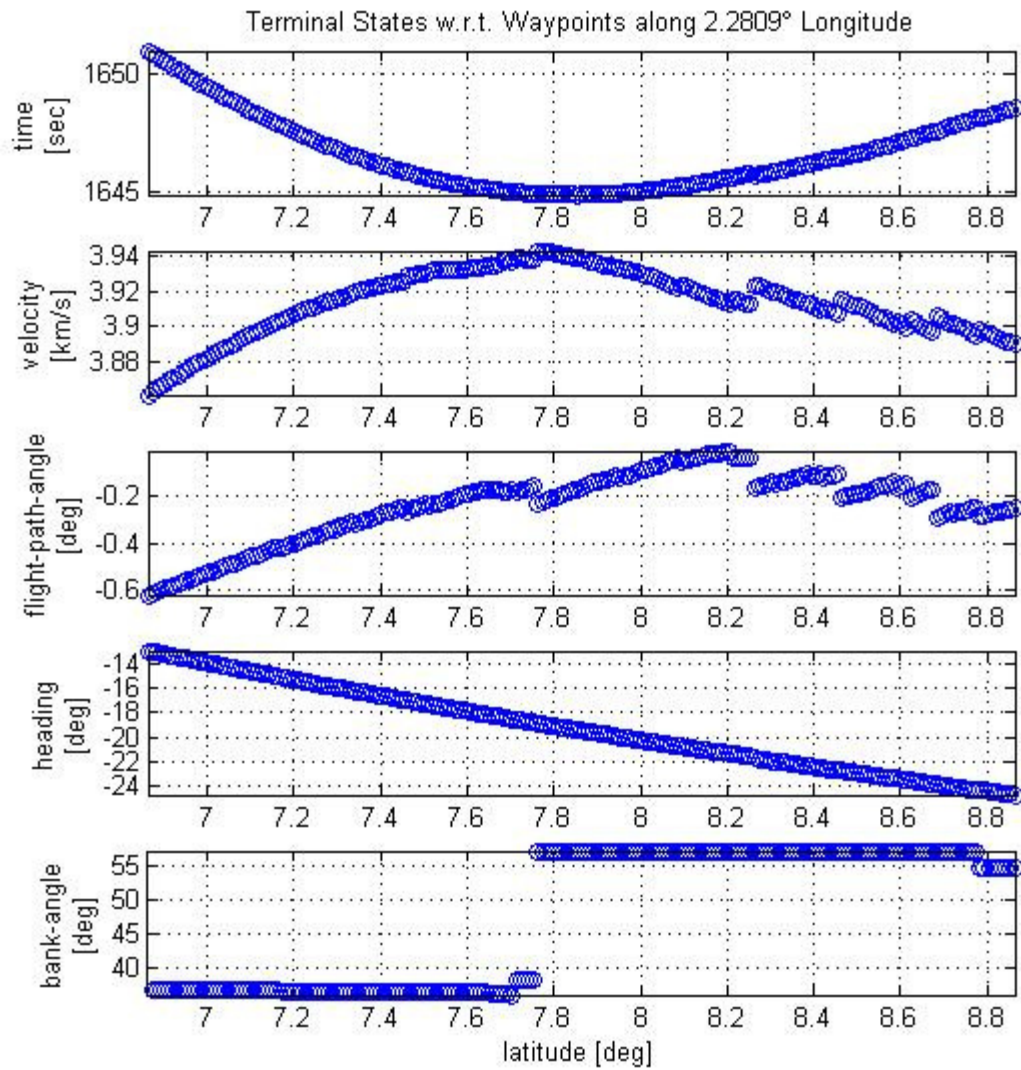
Figure 18. Case 1 terminal states with waypoints along longitude $2.2809°E$

As in the previous figures, but now more pronounced in Figure 18, the discontinuous breaks in the flight-path angle clearly correspond to the discontinuous breaks in the velocity.

The terminal states as depicted in the meridian slices (longitudinal variations in waypoint) show the parabolic nature of the terminal time and velocity associated with waypoints off the baseline trajectory. Additionally, the change in heading angle is approximately linear with waypoint displacement. Having demonstrated a technique to show the sensitivity on the terminal state for the non-rotating Earth, this technique and results are now expanded upon in cases 2 and 3.

4.4   Case 2 Results and Analysis

Case 2 presents a vehicle similar to case 1; however, case 2 differs from case 1 in: mass of the vehicle, inertial velocity and flight-path angle, due to the rotation rate of the Earth being turned 'on.' The optimal states are shown in Figure 19. As a note to furthering the discussion on rotation effects, we see that the two trajectories, case 1 and case 2, differ by approximately 400 seconds and a terminal speed of 2 km/s. Although a smaller portion of this difference is due to the difference in vehicle mass, the primary contribution is due to the difference in inertial velocities.

The surrounding area $0.5°$ (~30 nmi) north and south of the optimal nodes are sampled in increments of $0.01°$ (~0.6 nmi). Forty-three slices or families of waypoints composing a total of 3,640 evaluations of the surrounding field are compiled together to give the contours for terminal time and velocity. Figure 22 to Figure 24 are each a family of waypoints depicting their respective terminal states. As in case 1, the terminal time and velocity show strong parabolic shapes throughout. The discussion of the figures for cases 2 and 3 are very similar to that in case 1. Where appropriate, unique features will be discussed, but otherwise the reader is referred to case 1 Results and Analysis.
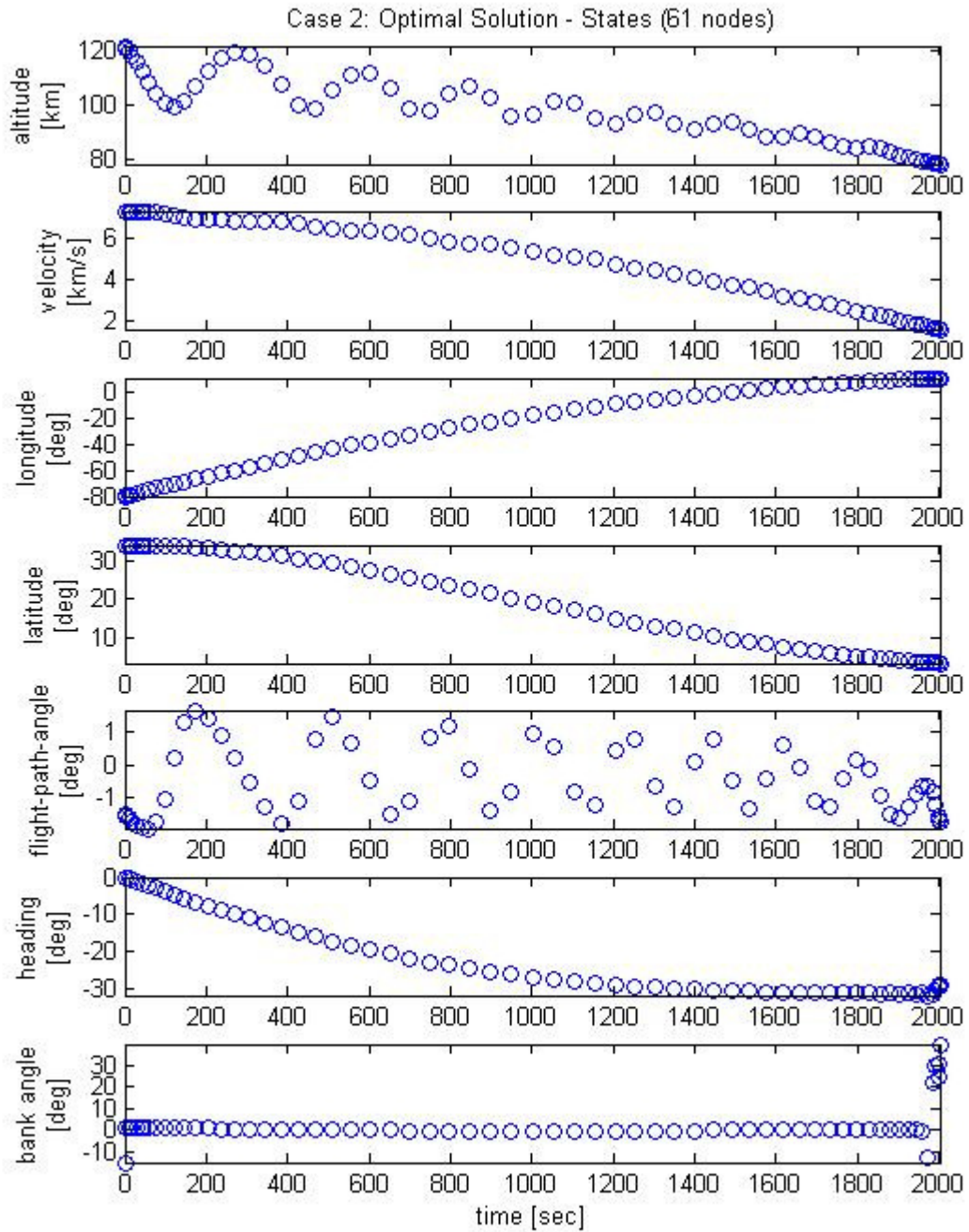
Figure 19. Case 2 results for the optimal solution without predefined waypoints.

Similar to the previous case, the RV performs a last minute bank maneuver to reduce the lift, and reach the target altitude.
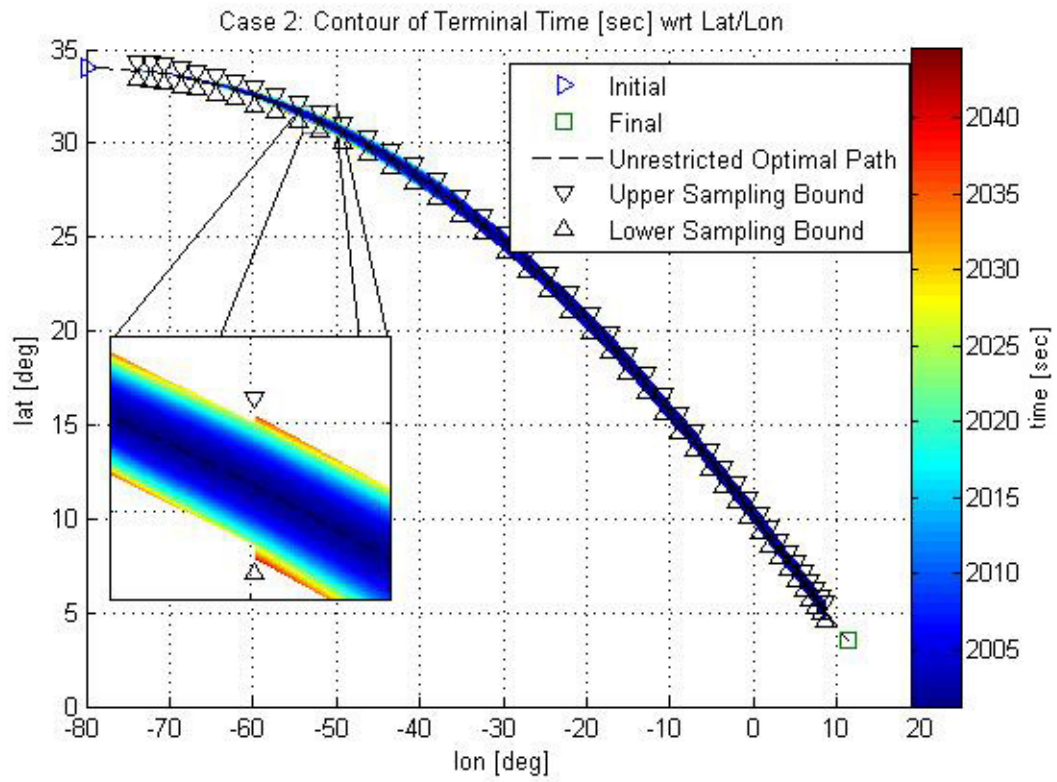
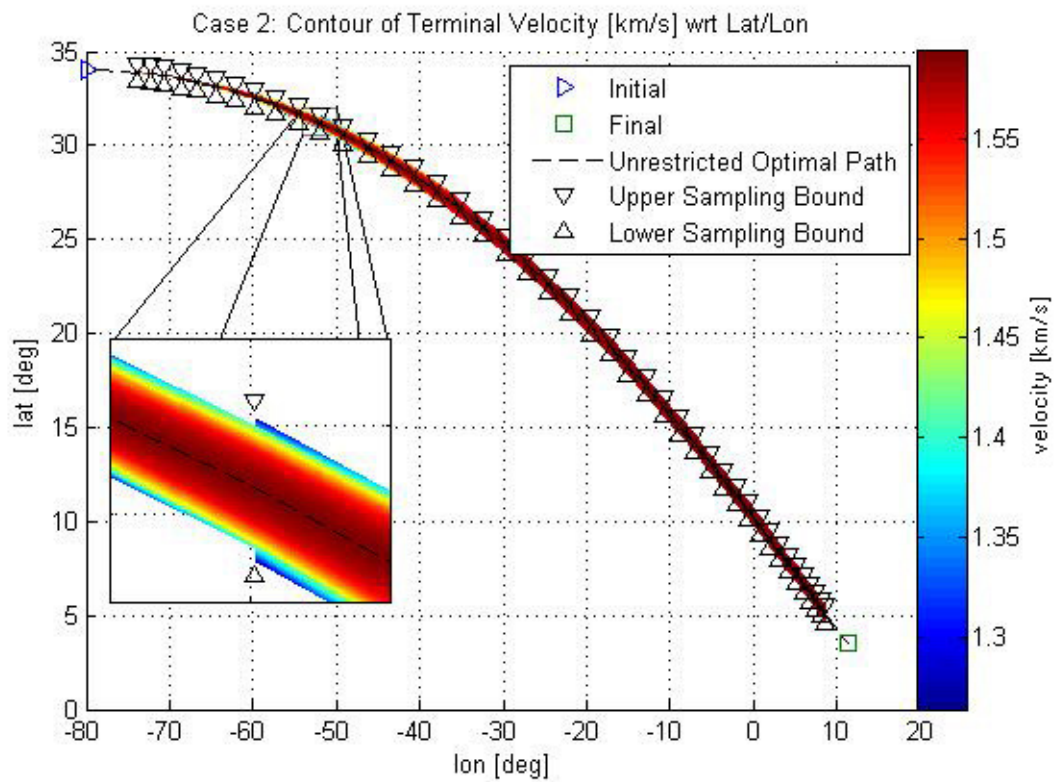**Figure 20.** Case 2 contour of terminal time w.r.t. Lat/Lon.

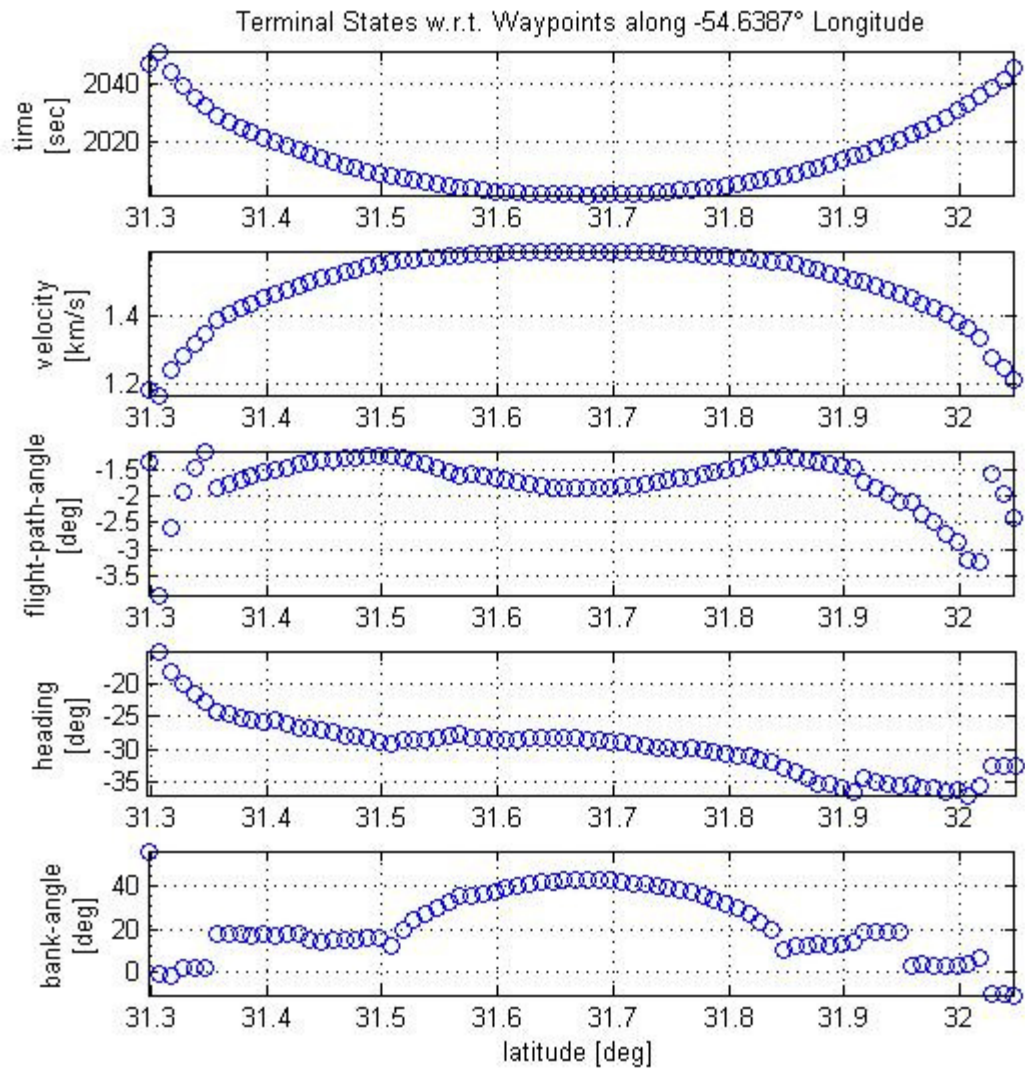**Figure 21.** Case 2 contour of terminal velocity w.r.t. Lat/Lon.

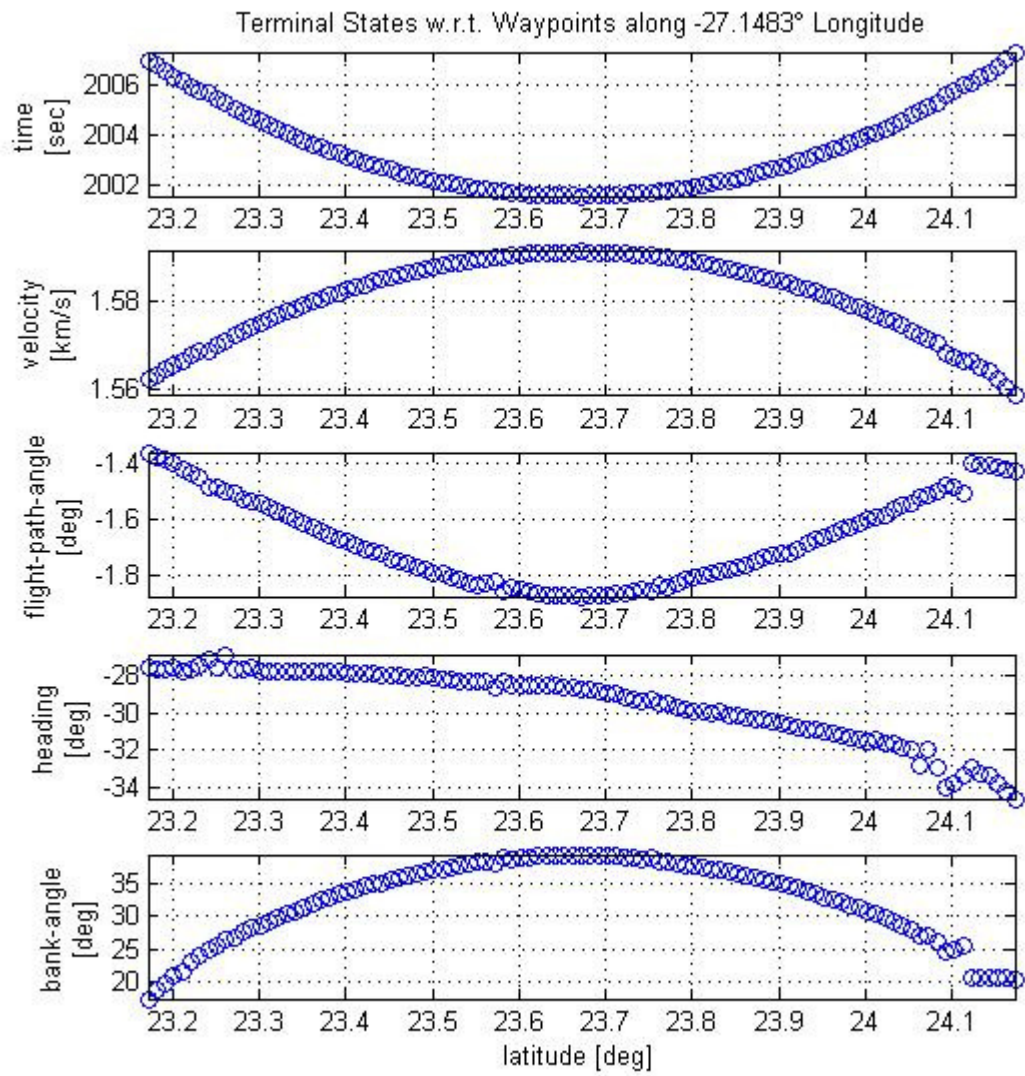**Figure 22.** Case 2 terminal states with waypoints along longitude -54.6387°E

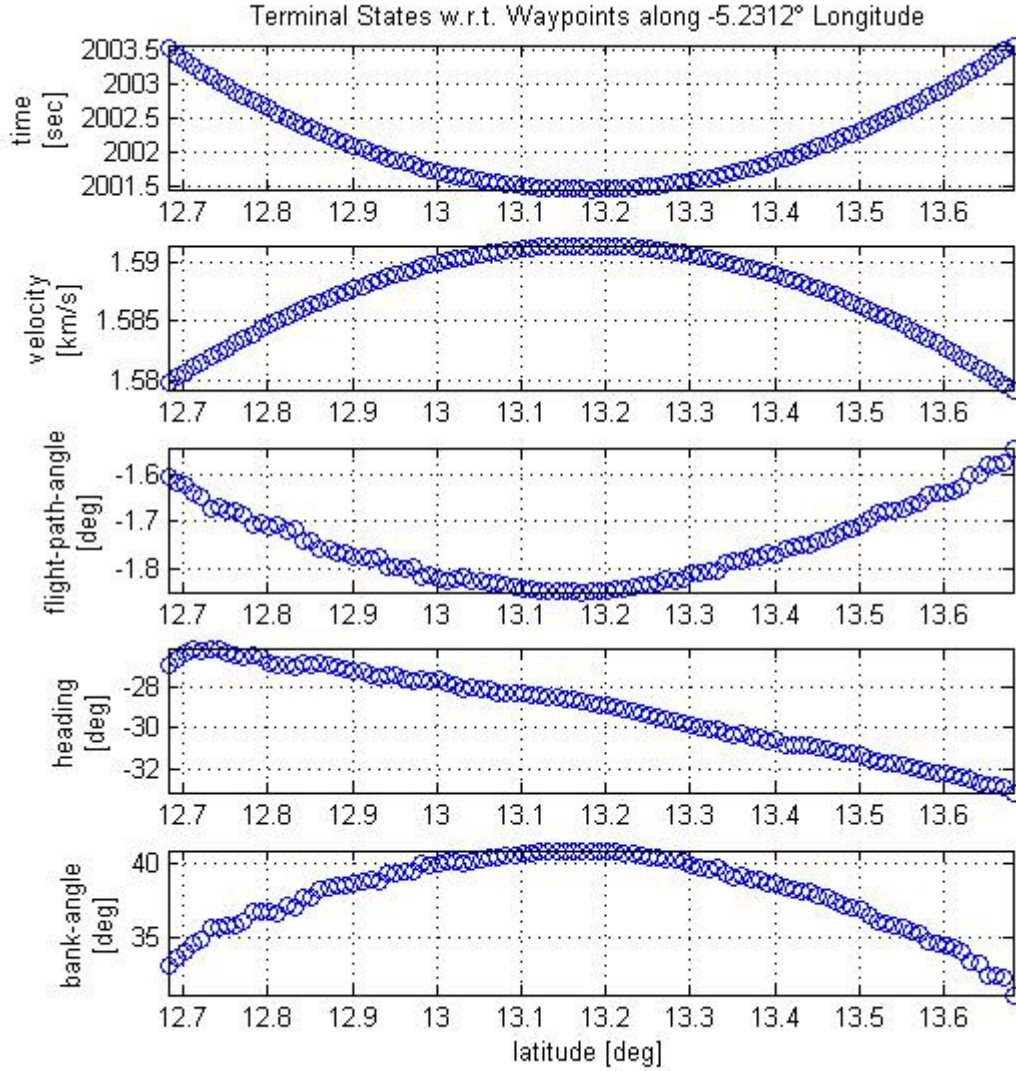**Figure 23.** Case 2 terminal states with waypoints along longitude $-27.1483°E$

Figure 24. Case 2 terminal states with waypoints along longitude $-5.2312°E$

Similar to case 1, the terminal states as depicted in the meridian slices show the parabolic nature of the terminal time and velocity associated with waypoints off the baseline trajectory. In contrast, the linearity of the heading angle used in case 1 appears to no longer exist. A mission planner may use Figure 24 to gain understanding how changing a waypoint affects the terminal state. In particular, the time and velocity are primary observables, whereas the other states are likely to significantly change which selection of subsequent waypoints.

4.5   *Case 3 Results and Analysis*

Case 3 is an extension of case 2. It addresses the question of how the trajectory sensitivity changes as waypoints are successively added, and put in the perspective of the mission planner, it answers the question, "Where else can the RV go?" In particular, case 3 has one predefined intermediate waypoint selected from the data collected in case 2. Figure 25 shows the selected waypoint slightly north of the nominal solution. Conveniently, the waypoint selected is a waypoint previously solved in case 2; therefore, the state history for the optimal solution through this waypoint is already obtained and shown in Figure 26.
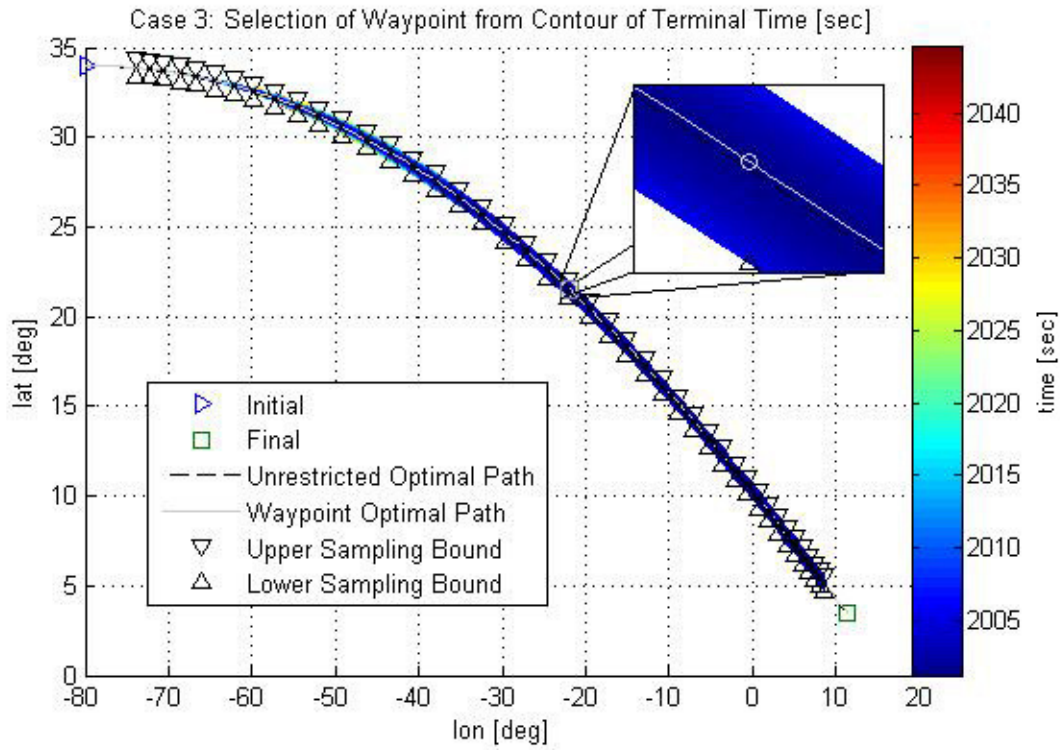

Figure 25. Case 3 selection of fixed waypoint.

The circle shown in the inset plot is the fixed waypoint $(-22.07° E, 21.59° N)$ that all the subsequent calculated trajectories will pass through.
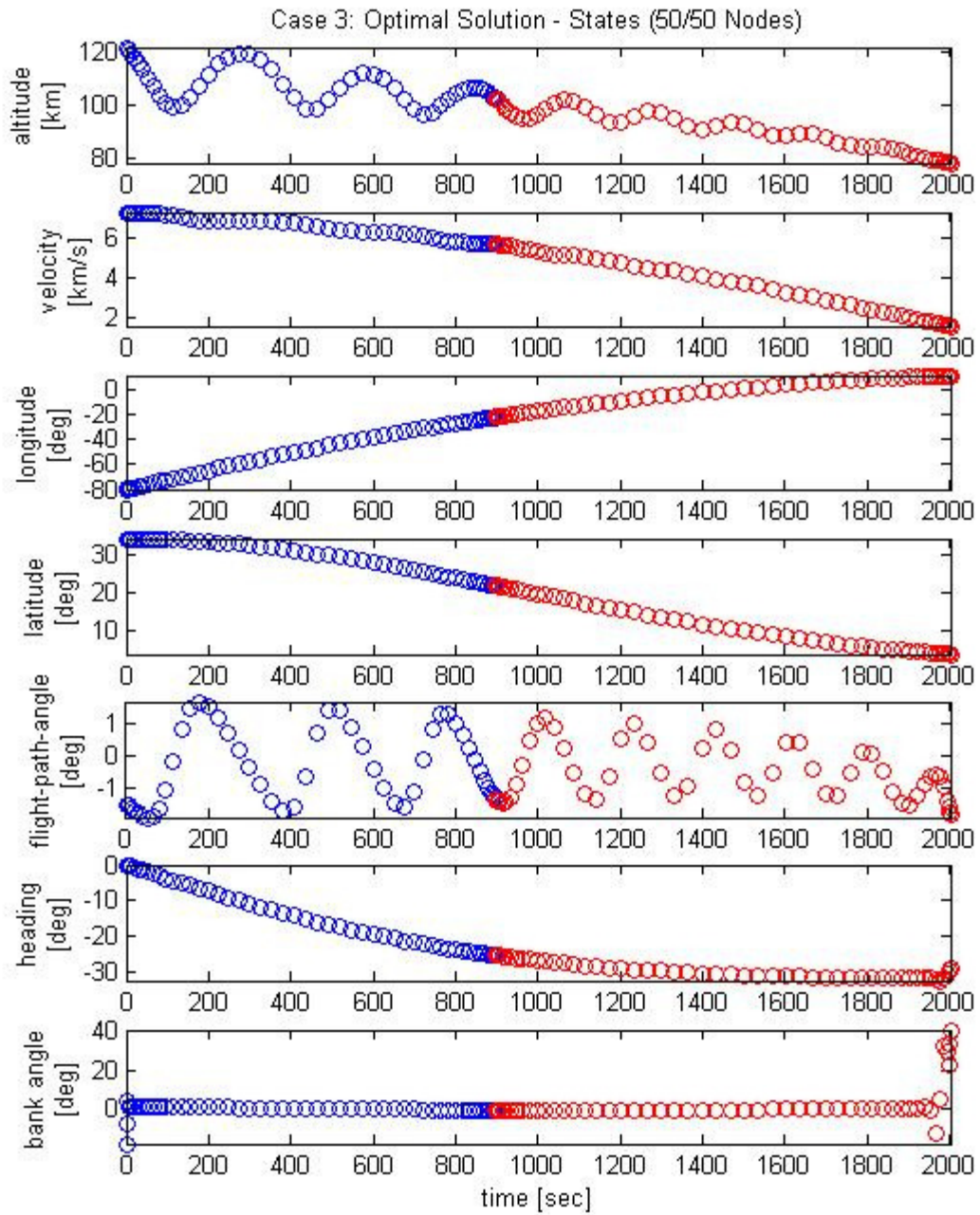
Figure 26. Case 3 results for the optimal solution with a predefined waypoint.

The optimal trajectory through the fixed waypoint is calculated with fifty nodes

in each phase of this two-phase solution represented by the blue and red circles.

The algorithm used to solve cases 1 and 2 is repeated here with the assumption that the waypoints are selected consecutively in time, so only the area following the waypoint is considered in the analysis. The results are presented in Figure 27 and Figure 28. These are the figures that would be most useful to a mission planner when the set of waypoints are overlaid thereby showing which waypoints are immediately feasible and what the cost is associated with flying through a particular waypoint.
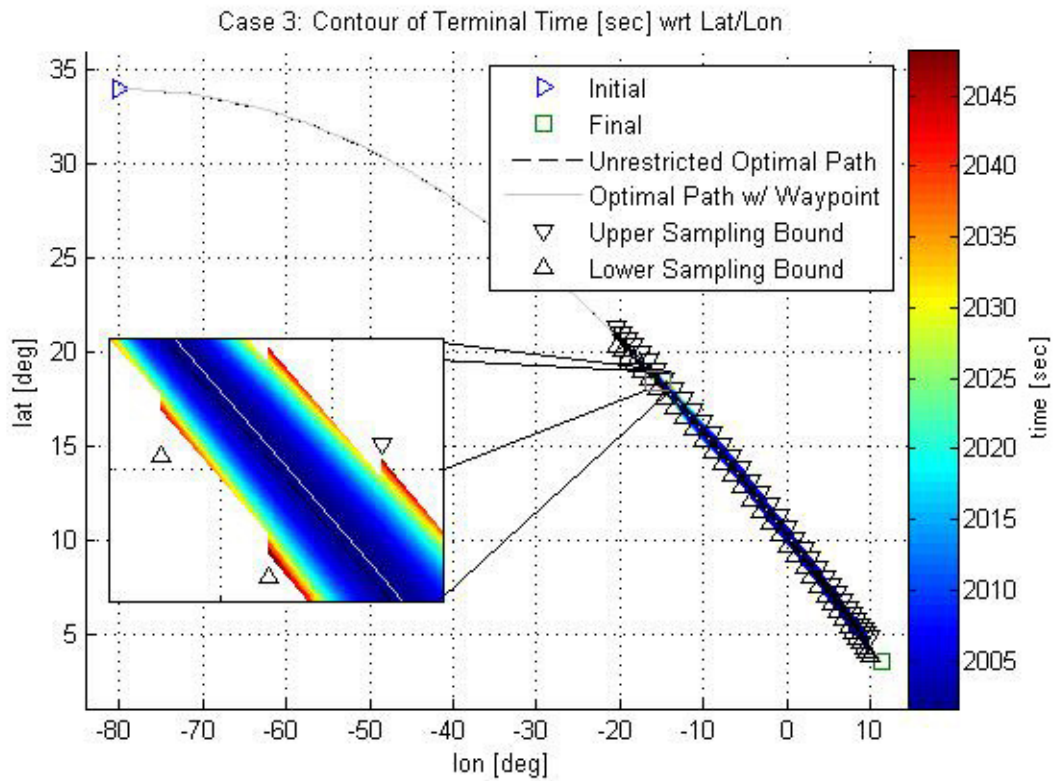

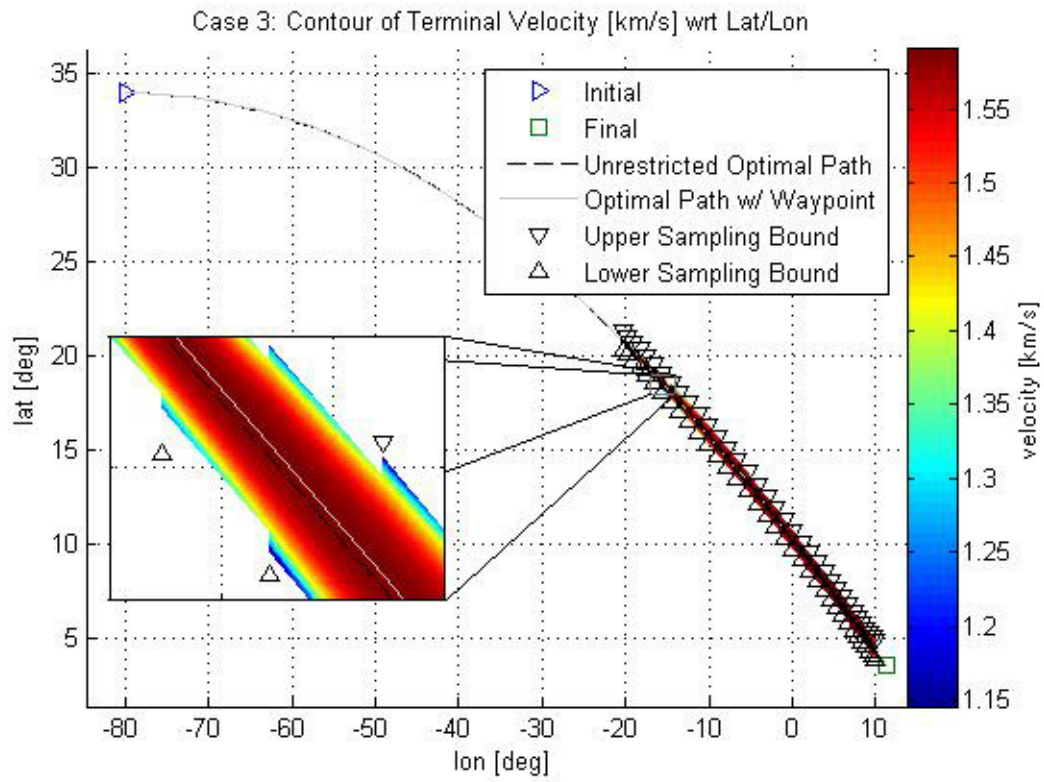**Figure 27.** Case 3 contour of terminal time w.r.t. Lat/Lon.

Figure 28. Case 3 contour of terminal velocity w.r.t. Lat/Lon.

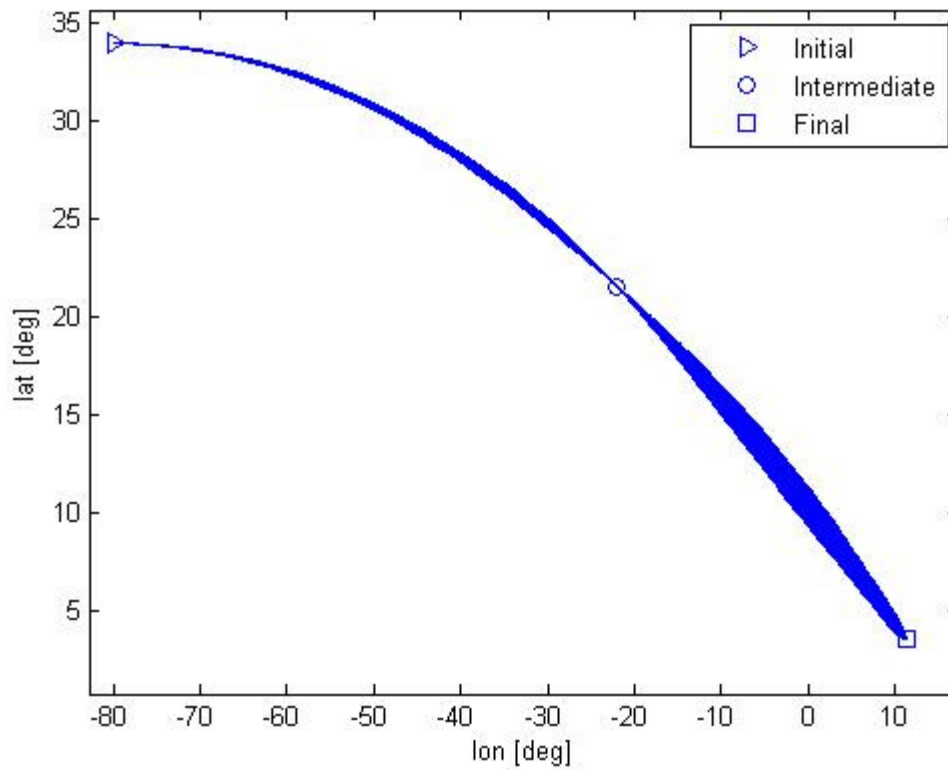**Figure 29.** Case 3 composite of all calculated trajectories.

Figure 29 is an 'aerial view' composite of all the trajectories. It depicts a bowtie looking silhouette with the trajectories all crossing at the fixed waypoint (as it must). Note, the altitude through the waypoint is not defined, so a 'side view' of the trajectories through the intermediate waypoint would show the RV ranging from 78 to 81 km in altitude.
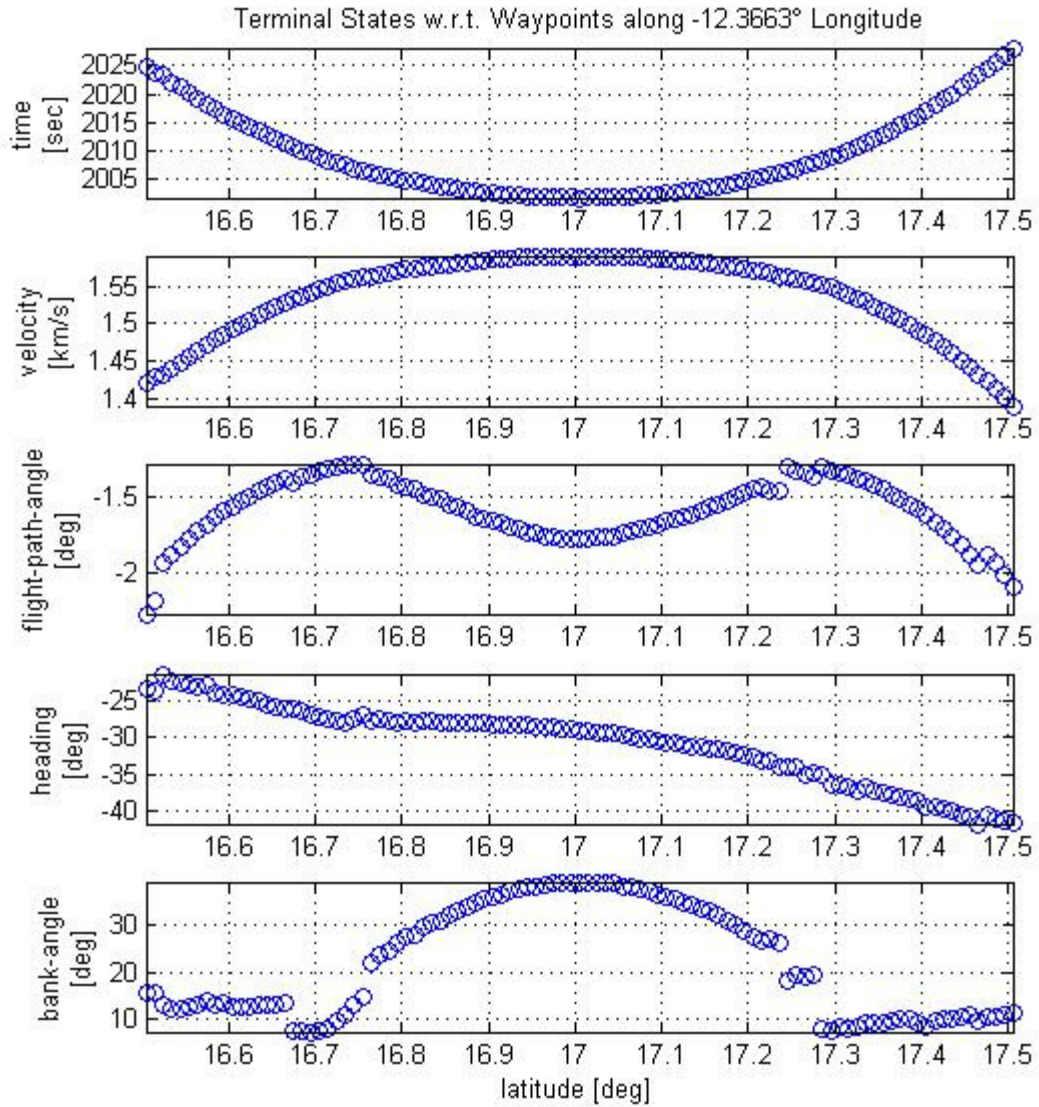
Figure 30. Case 3 terminal states with waypoints along longitude $-12.3663° E$

Like in the previous meridian slices, Figure 30 to Figure 32 show that the time

and velocity plots maintain a consistent parabolic shape. However, the flight-path angle

and bank angle plots are noticeably dissimilar from each other. In Figure 30, the flight-

path angle changes smoothly but has a peculiar region in which the curve's concavity

changes. In Figure 31, the flight-path angle is strictly concave up, and Figure 32 has

discontinuous breaks. Again, the interpretation and potential significance of these
curves are not yet understood.
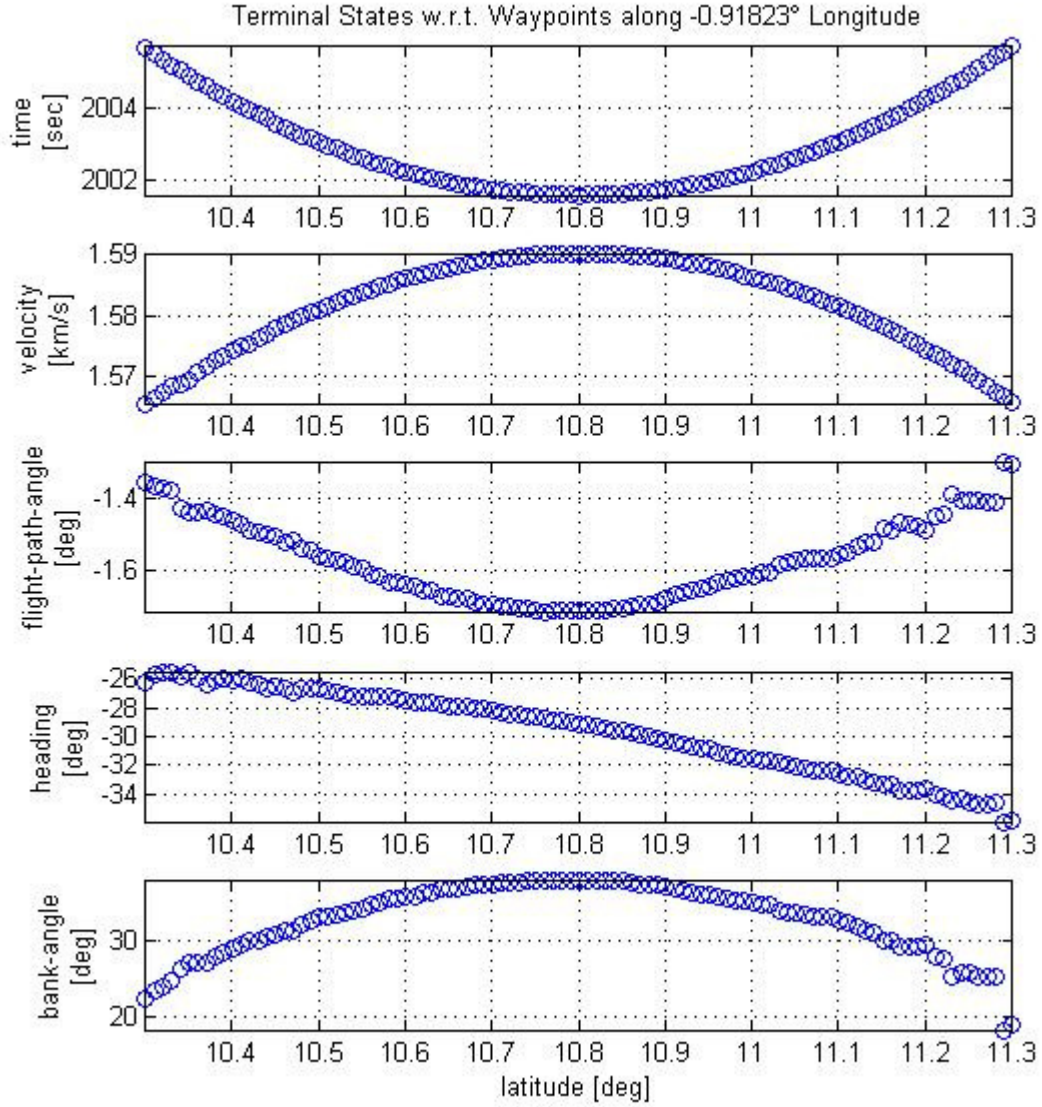
Figure 31. Case 3 terminal states with waypoints along longitude $-0.9182° E$
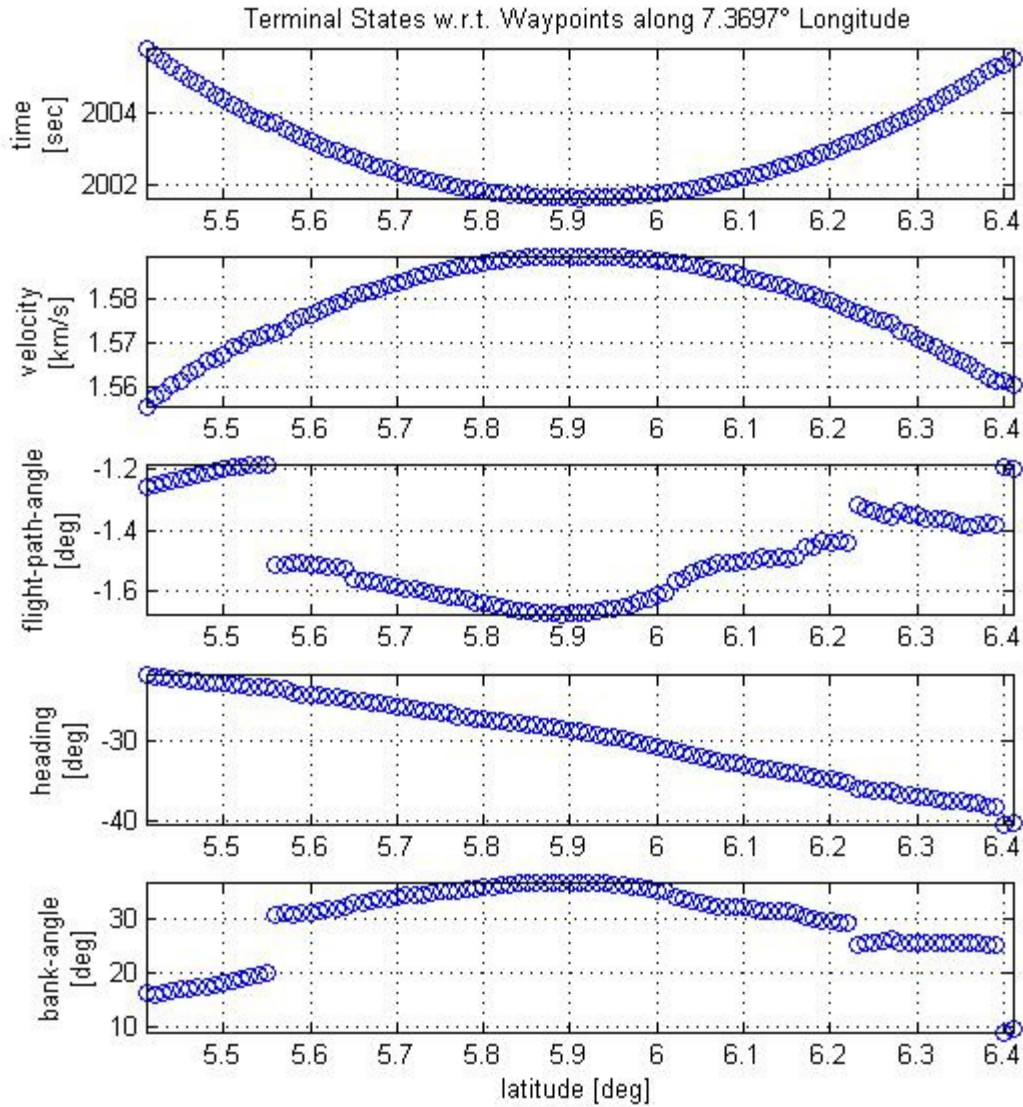
Figure 32. Case 3 terminal states with waypoints along longitude $7.3697° E$

The figures just presented are extremely useful to a mission planner. The contour plots, Figure 27 and Figure 28, identify regions where an RV can go and show the immediate cost associated with maneuvering to another waypoint. Figure 30 to Figure 32 focus on specific meridians that provide additional visual insight into trends in the data that are otherwise obscured by too much data. In the selection of additional

waypoints, the mission planner should consider small deviations in the trajectory that may significantly affect the terminal state. These terminal state characteristics are captured in the meridian slices which identify highly sensitive states through the discontinuous jumps in the data, e.g. the flight-path angle and bank angle at $5.55°$ latitude in Figure 32.

4.6 Finalizing Trajectory

This section makes some concluding observations applicable to any computed trajectory. For this analysis, a trajectory was selected that requires the RV to fly through two waypoints. The solution obtained is presented in Figure 33 where the state history is shown at discrete points in time. At approximately 1900 seconds, it appears that there is a discontinuous break in the bank angle data. However, the RV could rotate as fast as $\dot{\sigma} = \pm 60°/\sec$, as defined in Section 3.2.5. The spacing of the nodes around 1900 seconds prevents an adequate capture of the vehicle dynamics. A solution could be to simply fit a cubic polynomial through the data, propagate the initial state vector using the interpolated control data, and then compare to see if the two solutions match. Or, the problem can be re-solved using more nodes so that the vehicle dynamics are captured. The latter option has the benefit of improving the Hamiltonian, and therefore improving the overall optimality of the solution. Figure 34 shows the states again, but this time using four phases with ninety nodes in each. At approximately 1900 seconds, the bank angle no longer appears discontinuous. We also see in Figure 35 that the Hamiltonian for the four phase solution is more tightly packed to the optimal $H = -1$. The point of this last section is to further investigate some 'features' of the previous results. A numerical solution does not tell the whole truth, as might an analytical

solution. It is necessary to identify at what point in the trajectory the dynamics are not being adequately captured, and add additional nodes to fully capture the dynamics. A check of the Hamiltonian will verify that an optimal solution has been found. Figure 34 shows some additional detail of the dynamic behavior while Figure 35 illustrates the optimality of the results. This section builds confidence in the results of the earlier sections.

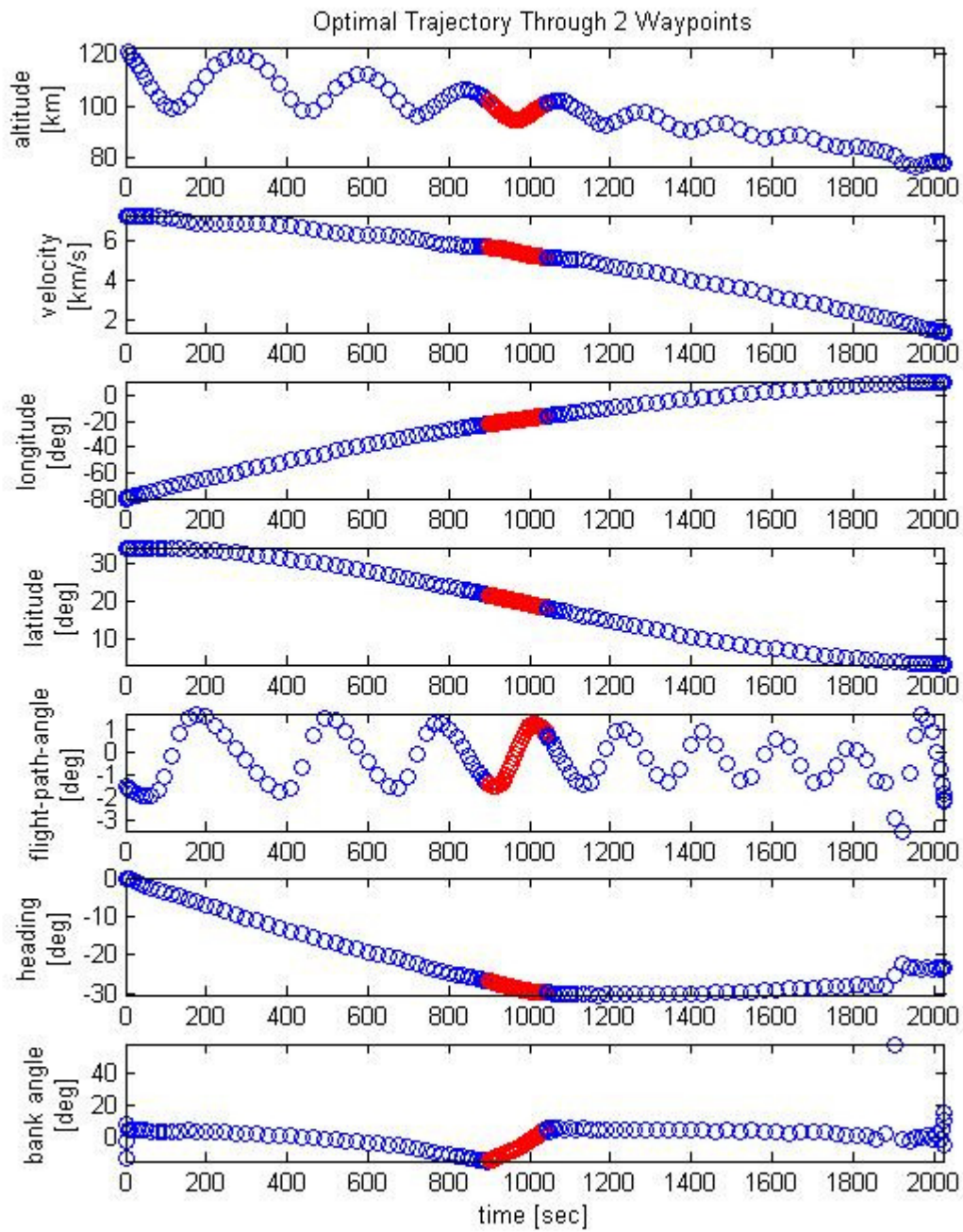**Figure 33.** Optimal trajectory through two waypoints represented by three phases (55-55-55 nodes).
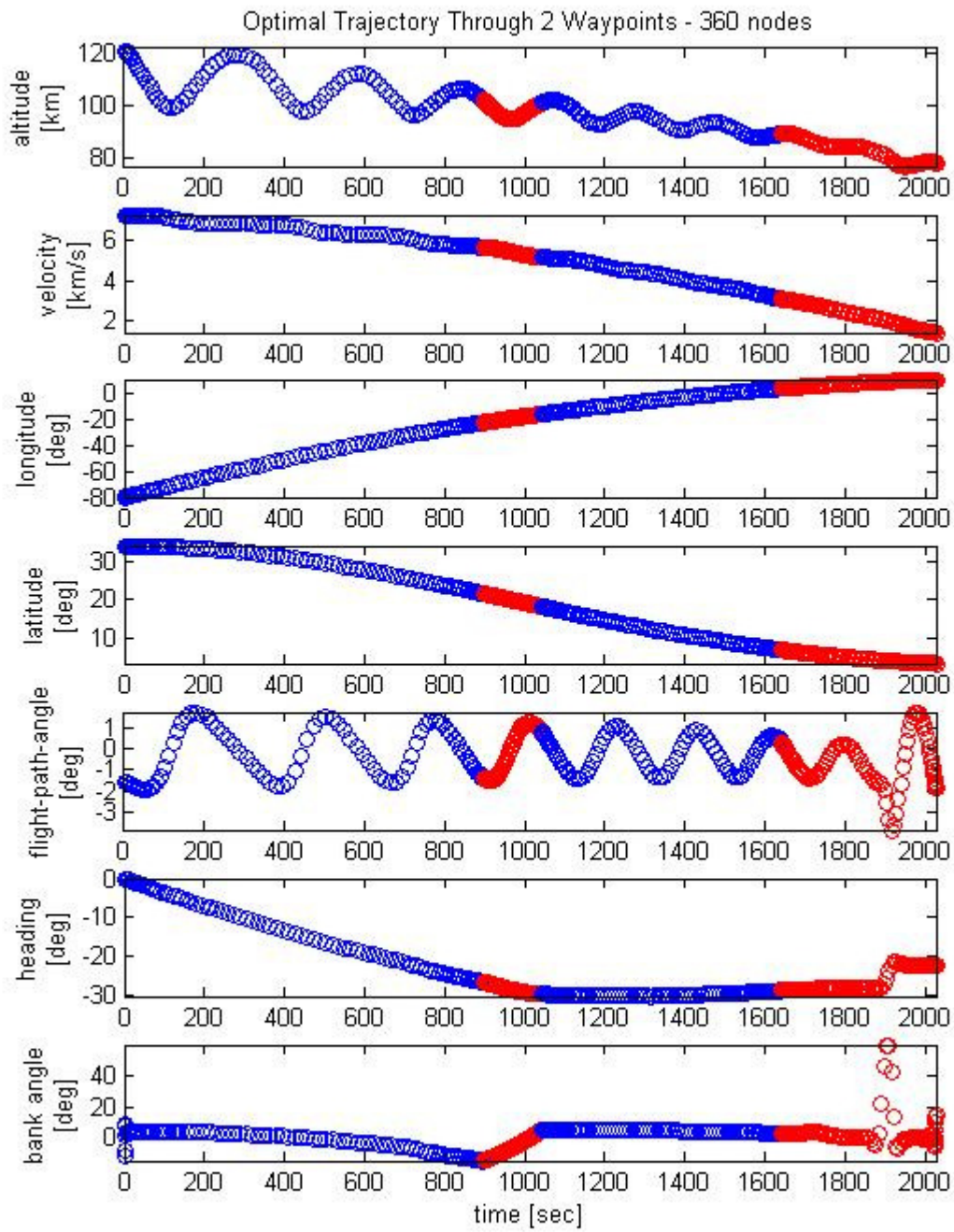
69

Figure 34. Optimal trajectory through two waypoints using four phases (90-90-90-90 nodes)
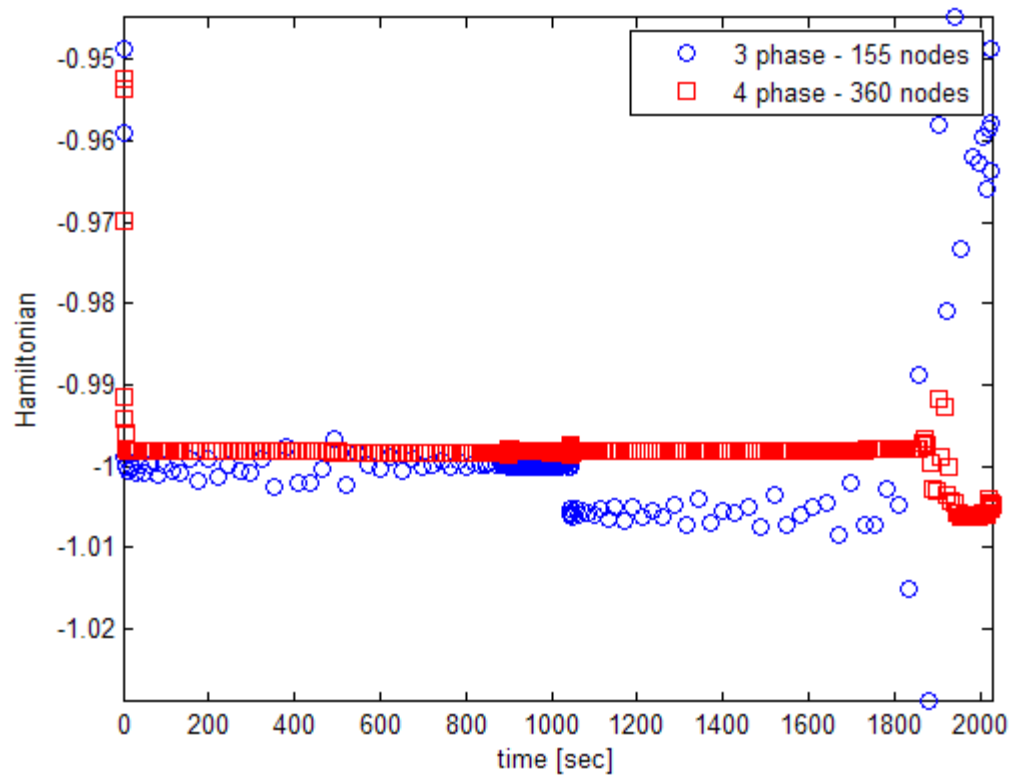
Figure 35. Hamiltonian of solution with 155 and 360 nodes.

4.7   Summary of Analysis

An incremental approach is taken to determine the sensitivity of the terminal

state to waypoint location. A minimum number of nodes used in the solutions is

established by propagating the initial conditions through an integrator and increasing

the nodes until the pseudospectral program output coincides with the integrated

solution. Comparing the footprints of straight, constant bank-angle flight trajectories

with the Earth rotation 'off' and 'on' justify the need to incorporate the Earth's rotation

rate into the equations of motion. After establishing an optimal trajectory between the

initial and final target, similar optimal control problems are solved with the restriction

that the RV passes through a nearby waypoint. Solving the optimal control problem at

numerous neighboring locations and tabulating the terminal state of each then describes

the sensitivity of the original optimal trajectory to changes in waypoint location. The

process was fully automated to select the neighboring waypoints, solve the optimal

trajectory for each waypoint, and then construct the contour plots. The changes to the

final state as a function of waypoint location are plotted for each case.

V. Conclusions and Future Work

5.1 Conclusions

In the course of solving the optimal control problem, this research built upon the already successful approach using GPM presented in [23] by including the spherical Earth model and the rotation rate of the Earth. With the addition of the new dynamics, it was realized that a 3D flat, non-rotating Earth is not suitable for accurately modeling shallow angle orbital re-entry problems. The increased model fidelity, however, also means abandoning absolute verification of the trajectory's optimality as analytical solutions are no longer available, although some assurance to the optimality can be gained by checking the Hamiltonian.

The introduction of uniformly spaced waypoints 'north' and 'south' of the nominal optimal trajectory serve to sample the surrounding field. Each waypoint location is a complete optimal control problem whereby a new optimal trajectory is computed, satisfying the waypoint and terminal constraints. Recognizing that the objective cost is the terminal time, comparing the terminal states of the baseline solution to the waypoint specified trajectories is a direct measurement of the system's sensitivity to waypoint location. The process was fully automated so that the user does not need to have knowledge of optimal control or need to manually select waypoints. Even with automation, computation time for problems presented in this research (each case) ranged from three to ten days on a Pentium dual core 32-bit 2 GHz processor.

5.2 Future Work

There are four main avenues of future work: continue increasing the model fidelity to the re-entry vehicle and environment, expand the sampling region to include

all feasible solutions, add additional features for specific mission requirements, and seek faster solutions.

Obvious enhancements to model fidelity include applying the heating constraint, using angle-of-attack as a control, and C_L and C_D as a function of angle-of-attack. These three modifications would round out the basic model for any generic re-entry vehicle. Once the vehicle is well-defined, other considerations such as using better atmospheric and Earth models are within reason. Beyond these suggestions is an exercise in applying corrections on top of corrections.

It is assumed that the range of all feasible solutions is continuous within an enclosed envelope surrounding the nominal trajectory. This research, although not focused on finding the extreme upper and lower boundaries, has provisions to continue until unable to continue further. At each slice, the algorithm is instructed to stop proceeding after a maximum number of increments or an infeasible solution is reached. If the maximum iteration limit restriction is lifted, an upper and lower bound of feasible solutions along each slice is, in theory, obtainable. The 'stop' conditions mentioned earlier resulted in the program terminating too soon. Aside from the normal 'stop' conditions, the event may be triggered by too large a step size, a poor initial guess at the solution, or a hypothetical infeasible region contained within the envelope of all feasible solutions. Results presented in Chapter IV suggest such infeasible regions may exist; therefore, future work in identifying the region of all feasible waypoints should also answer the question about infeasible regions.

A mission feature omitted from this research but included in Maj Jorris' dissertation is the presence of no-fly zones built directly into the optimization problem.

Therefore the reincorporation of no-fly zones and previously recommended future work from [23] are certainly viable.

The initial algorithm and design for this research was laid out early on under the assumption that sampling the field at many points would not take very long to compute. This decision was due to expectations set by the method converging to an optimal solution in seconds from the work conducted in [23]. The algorithm presented in Figure 7 is constructed in such a way that adaptation to a distributed or parallel computing system is feasible. Obtaining results quicker than the last is always heralded as a good achievement, and so future research should seek to reduce the computation time (in lieu of processor speed advancements) by means such as algorithmic changes, problem reformulation, and efficient coding.

Appendix A. Non-dimensionalization

A.1   *Non-dimensional 3-D Re-entry Equations of Motion – Rotating Earth*

The 3D equations of motion from [20], omitting the thrust terms, are:

$$\dot{r} = {}^{R}V \sin \gamma \tag{A.1}$$

$$\dot{\theta} = \frac{{}^{R}V \cos \gamma \cos \psi}{r \cos \phi} \tag{A.2}$$

$$\dot{\phi} = \frac{{}^{R}V \cos \gamma \sin \psi}{r} \tag{A.3}$$

$$^{R}\dot{V} = -\frac{D}{m} - g \sin \gamma + r\omega_{\oplus}^{2} \cos \phi \left(\cos \phi \sin \gamma - \sin \phi \sin \psi \cos \gamma \right) \tag{A.4}$$

$$\dot{\gamma} = \frac{L}{{}^{R}Vm} \cos \sigma - \frac{g}{{}^{R}V} \cos \gamma + \frac{{}^{R}V}{r} \cos \gamma + 2\omega_{\oplus} \cos \phi \cos \psi + \dots$$
$$\dots + \frac{r\omega_{\oplus}^{2}}{{}^{R}V} \cos \phi \left(\cos \phi \cos \gamma + \sin \phi \sin \psi \sin \gamma \right) \tag{A.5}$$

$$\dot{\psi} = \frac{L \sin \sigma}{{}^{R}Vm \cos \gamma} - \frac{{}^{R}V}{r} \cos \gamma \cos \psi \tan \phi + 2\omega_{\oplus} \left(\sin \psi \cos \phi \tan \gamma - \sin \phi \right) \dots$$
$$\dots - \frac{r\omega_{\oplus}^{2}}{{}^{R}V \cos \gamma} \sin \phi \cos \phi \cos \psi \tag{A.6}$$

Non-dimensionalize the equations using:

$$r' = \frac{r}{r_0} \tag{A.7}$$

$$^{R}V' = \frac{{}^{R}V}{\sqrt{g_0 r_0}} \tag{A.8}$$

$$\tau = \frac{t}{\sqrt{r_0 / g_0}} \tag{A.9}$$

$$L' = \frac{L}{g_0 m} \tag{A.10}$$

$$D' = \frac{D}{g_0 m} \tag{A.11}$$

Note gravity is a function of r, and can be rewritten in terms of the new non-dimensional

term r' .

$$g = g_0 \left(\frac{r_0}{r} \right)^2 = \frac{g_0}{r'^2} \tag{A.12}$$

Also the rotation rate of the Earth, $\omega_\oplus$, needs to be non-dimensionalized which can be

achieved by multiplying by $\sqrt{r_0 / g_0}$. Therefore we now have:

$$\omega'_\oplus = \omega_\oplus \sqrt{r_0 / g_0} \tag{A.13}$$

Now the non-dimensional equations of motion can be derived:

Radial Distance:

$$\frac{dr'}{d\tau} = \frac{d\left(r/r_0\right)}{d\left(t / \sqrt{r_0 / g_0}\right)} = \frac{1}{\sqrt{r_0 g_0}} \frac{dr}{dt} \tag{A.14}$$

$$\frac{dr'}{d\tau} = \frac{1}{\sqrt{r_0 g_0}} \left[{}^R V \sin \gamma \right] \tag{A.15}$$

$$\boxed{\frac{dr'}{d\tau} = {}^R V' \sin \gamma} \tag{A.16}$$

Velocity:

$$\frac{d\,^{R}V'}{d\tau} = \frac{d\left(\,^{R}V\big/\sqrt{g_0 r_0}\right)}{d\left(t\big/\sqrt{r_0\big/g_0}\right)} = \frac{1}{\sqrt{g_0 r_0}}\sqrt{\frac{r_0}{g_0}}\frac{d\,^{R}V}{dt} = \frac{1}{g_0}\frac{d\,^{R}V}{dt} \tag{A.17}$$

$$\frac{d\,^{R}V'}{d\tau} = \frac{1}{g_0}\left[-\frac{D}{m} - g\sin\gamma + r\omega_{\oplus}^2\cos\phi\left(\cos\phi\sin\gamma - \sin\phi\sin\psi\cos\gamma\right)\right] \tag{A.18}$$

$$\boxed{\frac{d\,^{R}V'}{d\tau} = -\frac{\sin\gamma}{r'^2} + r'\omega_{\oplus}'^2\cos\phi\left(\cos\phi\sin\gamma - \sin\phi\sin\psi\cos\gamma\right) - D'} \tag{A.19}$$

Longitude:

$$\frac{d\theta'}{d\tau} = \frac{d\theta}{d\left(t\big/\sqrt{r_0\big/g_0}\right)} = \sqrt{\frac{r_0}{g_0}}\frac{d\theta}{dt} \tag{A.20}$$

$$\frac{d\theta'}{d\tau} = \sqrt{\frac{r_0}{g_0}}\left[\frac{\,^{R}V\cos\gamma\cos\psi}{r\cos\phi}\right] \tag{A.21}$$

$$\boxed{\frac{d\theta'}{d\tau} = \left(\frac{\,^{R}V'}{r'}\right)\frac{\cos\gamma\cos\psi}{\cos\phi}} \tag{A.22}$$

Latitude:

$$\frac{d\phi'}{d\tau} = \frac{d\phi}{d\left(t\big/\sqrt{r_0\big/g_0}\right)} = \sqrt{\frac{r_0}{g_0}}\frac{d\phi}{dt} \tag{A.23}$$

$$\frac{d\phi'}{d\tau} = \sqrt{\frac{r_0}{g_0}}\left[\frac{\,^{R}V\cos\gamma\sin\psi}{r}\right] \tag{A.24}$$

$$\boxed{\frac{d\phi'}{d\tau} = \left(\frac{\,^{R}V'}{r'}\right)\cos\gamma\sin\psi} \tag{A.25}$$

Flight-path-angle:

$$\frac{d\gamma'}{d\tau} = \frac{d\gamma}{d\left(t \middle/ \sqrt{r_0 \middle/ g_0} \right)} = \sqrt{\frac{r_0}{g_0}} \frac{d\gamma}{dt} \tag{A.26}$$

$$\frac{d\gamma'}{d\tau} = \sqrt{\frac{r_0}{g_0}} \left[\frac{L}{^R V m} \cos\sigma - \frac{g}{^R V} \cos\gamma + \frac{^R V}{r} \cos\gamma + 2\omega_\oplus \cos\phi \cos\psi \right] + \ldots$$
$$\ldots + \sqrt{\frac{r_0}{g_0}} \frac{r\omega_\oplus^2}{^R V} \cos\phi \left(\cos\phi \cos\gamma + \sin\phi \sin\psi \sin\gamma \right) \tag{A.27}$$

$$\boxed{\begin{aligned} \frac{d\gamma'}{d\tau} &= \frac{L'}{^R V'} \cos\sigma - \frac{\cos\gamma}{r'^2 \, ^R V'} + \frac{^R V'}{r'} \cos\gamma + 2\omega'_\oplus \cos\phi \cos\psi + \ldots \\ &\ldots + \frac{r'}{^R V'} \omega'^2_\oplus \cos\phi \left(\cos\phi \cos\gamma + \sin\phi \sin\psi \sin\gamma \right) \end{aligned}} \tag{A.28}$$

Heading:

$$\frac{d\psi'}{d\tau} = \frac{d\psi}{d\left(t \middle/ \sqrt{r_0 \middle/ g_0} \right)} = \sqrt{\frac{r_0}{g_0}} \frac{d\psi}{dt} \tag{A.29}$$

$$\frac{d\psi'}{d\tau} = \sqrt{\frac{r_0}{g_0}} \left[\frac{L \sin\sigma}{^R V m \cos\gamma} - \frac{^R V}{r} \cos\gamma \cos\psi \tan\phi + 2\omega_\oplus \left(\sin\psi \cos\phi \tan\gamma - \sin\phi \right) \right] \ldots$$
$$\ldots - \sqrt{\frac{r_0}{g_0}} \frac{r\omega_\oplus^2}{^R V \cos\gamma} \sin\phi \cos\phi \cos\psi \tag{A.30}$$

$$\boxed{\begin{aligned} \frac{d\psi'}{d\tau} &= \frac{L' \sin\sigma}{^R V' \cos\gamma} - \frac{^R V'}{r'} \cos\gamma \cos\psi \tan\phi + 2\omega'_\oplus \left(\sin\psi \cos\phi \tan\gamma - \sin\phi \right) \ldots \\ &\ldots - \frac{r'\omega'^2_\oplus}{^R V'} \frac{\sin\phi \cos\phi \cos\psi}{\cos\gamma} \end{aligned}} \tag{A.31}$$

The atmosphere is modeled as a simple exponential.

$$\rho = \rho_0 e^{-\beta(r - r_0)} \tag{A.32}$$

And therefore lift can be rewritten

$$L = \frac{\rho C_L S\, {}^R V^2}{2} = \frac{\rho_0 e^{-\beta(r-r_0)} C_L S\, {}^R V^2}{2}$$

(A.33)

$$L = \frac{\rho_0 e^{-\beta(r'r_0-r_0)} C_L S\, {}^R V'^2 g_0 r_0}{2} = \frac{\rho_0 e^{-\beta r_0(r'-1)} C_L S\, {}^R V'^2 g_0 r_0}{2}$$

(A.34)

And dividing by $g_0 m$

$$L' = \frac{L}{g_0 m} = \frac{\rho_0 e^{-\beta r_0(r'-1)} C_L S\, {}^R V'^2 g_0 r_0}{2 g_0 m}$$

(A.35)

$$\boxed{L' = \frac{\rho_0 e^{-\beta r_0(r'-1)} C_L S\, {}^R V'^2 r_0}{2m}}$$

(A.36)

Similarly drag is:

$$\boxed{D' = \frac{\rho_0 e^{-\beta r_0(r'-1)} C_D S\, {}^R V'^2 r_0}{2m}}$$

(A.37)

In summary the non-dimensional equations of motion are (A.16),(A.19),(A.22),(A.25),

(A.28),(A.31) respectively:

$$\frac{dr'}{d\tau} = {}^R V' \sin\gamma$$

$$\frac{d\,{}^R V'}{d\tau} = -\frac{\sin\gamma}{r'^2} + r'\omega_\oplus'^2 \cos\phi\left(\cos\phi\sin\gamma - \sin\phi\sin\psi\cos\gamma\right) - D'$$

$$\frac{d\theta'}{d\tau} = \left(\frac{{}^R V'}{r'}\right)\frac{\cos\gamma\cos\psi}{\cos\phi}$$

$$\frac{d\phi'}{d\tau} = \left(\frac{{}^R V'}{r'}\right)\cos\gamma\sin\psi$$

$$\frac{d\gamma'}{d\tau} = \frac{L'}{{}^R V'}\cos\sigma - \frac{\cos\gamma}{r'^2\,{}^R V'} + \frac{{}^R V'}{r'}\cos\gamma + 2\omega_\oplus'\cos\phi\cos\psi + \frac{r'}{{}^R V'}\omega_\oplus'^2\cos\phi\left(\cos\phi\cos\gamma + \sin\phi\sin\psi\sin\gamma\right)$$

$$\frac{d\psi'}{d\tau} = \frac{L'\sin\sigma}{{}^R V'\cos\gamma} - \frac{{}^R V'}{r'}\cos\gamma\cos\psi\tan\phi + 2\omega_\oplus'\left(\sin\psi\cos\phi\tan\gamma - \sin\phi\right) - \frac{r'\omega_\oplus'^2}{{}^R V'}\frac{\sin\phi\cos\phi\cos\psi}{\cos\gamma}$$

Appendix B. MATLAB® Function Descriptions

Several MATLAB® scripts and functions are used in the course of this research.
The files are categorized into: problem setup, files required by OPENPOCS, and
graphics output. A MATLAB® function has the form:

[output] = function_name (input)

and can accept multiple inputs and outputs. A script file unlike a function does not
require any input, but all of the executed code contained in the script is available to the
calling function.

B.1   Problem Setup

```
main.m
    ├ design_problem.m
    ├ combine.m
    ├ findsoln_ic2fc.m
    │          └ workhorse.m
    │                     ├ design_parameters.m
    │                     └ <OPENPOCS>
    └findsoln_ic2wp2fc.m
               ├ workhorse2.m
               │     ├design_parameters.m
               │     └ <OPENPOCS>
               └workhorse3.m
                     ├ design_parameters.m
                     └ <OPENPOCS>
```
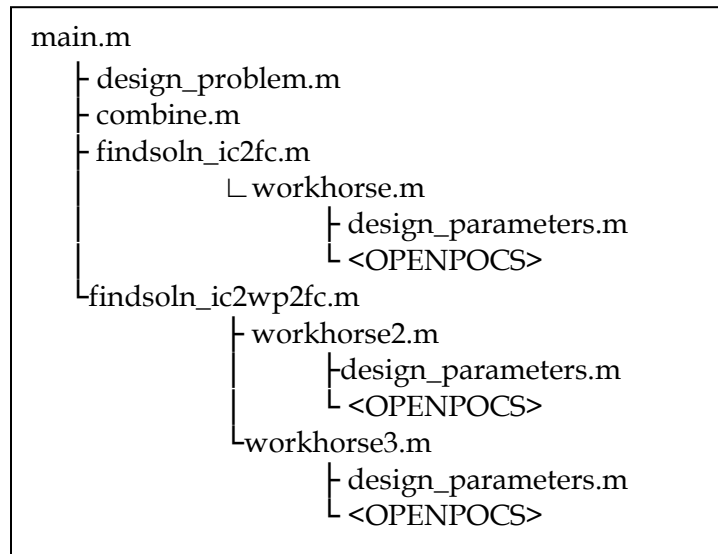
Figure 36. Program directory tree.

- **main.m**: This is a script file that initializes and ties together all the subfunctions

  used in calculating the optimal trajectories.

- **design_problem.m**: This script file contains the initial, intermediate (optional),

  and final conditions.

- **combine.m**: This function file receives as input the initial, intermediate (optional), and final conditions defined in *design_problem.m*, and combines them into a single structure.

- **findsoln_ic2fc.m**: This function computes the unrestricted optimal solution between the initial and final target.

- **workhorse.m**: This function calculates the one-phase optimal trajectory between the initial and final target.

- **design_parameters.m**: This is a script file that contains constants for the model, vehicle, and scaling factors.

- **findsoln_ic2wp2fc.m**: This function splits the one-phase optimal solution obtained in findsoln_ic2fc.m into two-phase solutions and selects waypoints used in mapping the sensitivity contours.

- **workhorse2.m**: This function calculates the two-phase optimal trajectory between the initial and final target with an intermediate waypoint specified.

- **workhorse3.m**: This function calculates the three-phase optimal trajectory between the initial and final target with two intermediate waypoints specified.

B.2   *Files Required By OPENPOCS*

- **cost_mintime_openpocs.m**: This function contains the objective cost function.

- **eom_hicks_nd_openpocs.m**: This function contains the equations of motion and path constraints.

- **connection_openpocs.m**: This function specifies how the phases link to eachother.

B.3 Graphics Output

- **printsoln.m**: This function prints the state history of a specific trajectory.

- **printcontours.m**: This function prints the terminal time and velocity contours.

Appendix C. Coordinate Transformations

C.1   *Earth Centered Inertial to Earth Centered Earth Fixed*

The following are the steps required to convert from the Earth Centered Inertial (ECI) to the Earth Centered Earth Fixed Frame (ECEF) using the following inertial state vector:

$$\begin{bmatrix} r \\ V \\ \theta \\ \phi \\ \gamma \\ \psi \end{bmatrix} \tag{C.1}$$

Convert position in inertial frame from spherical coordinates to the Cartesian coordinates.

$$\begin{bmatrix} x \\ y \\ z \end{bmatrix} = \begin{bmatrix} r\cos(\phi)\cos(\theta) \\ r\cos(\phi)\sin(\theta) \\ r\sin(\phi) \end{bmatrix} \tag{C.2}$$

Likewise, convert the velocity from spherical to Cartesian, i.e. the east-north-up frame.

$$\begin{bmatrix} V_e \\ V_n \\ V_u \end{bmatrix} = \begin{bmatrix} V\cos(\gamma)\cos(\psi) \\ V\cos(\gamma)\sin(\psi) \\ V\sin(\gamma) \end{bmatrix} \tag{C.3}$$

Then convert the velocity to the inertial frame. This is accomplished by a Body Three 2-3 rotation. (Note: the coordinates e-n-u are re-arranged to u-e-n)

$$\begin{bmatrix} V_x \\ V_y \\ V_z \end{bmatrix} = \begin{bmatrix} \cos(-\theta) & \sin(-\theta) & 0 \\ -\sin(-\theta) & \cos(-\theta) & 0 \\ 0 & 0 & 1 \end{bmatrix} \begin{bmatrix} \cos(\phi) & 0 & -\sin(\phi) \\ 0 & 1 & 0 \\ \sin(\phi) & 0 & \cos(\phi) \end{bmatrix} \begin{bmatrix} V_u \\ V_e \\ V_n \end{bmatrix} \tag{C.4}$$

The velocity due to Earth's rotation is subtracted.

$$\begin{bmatrix} V_x \\ V_y \\ V_z \end{bmatrix} = \begin{bmatrix} V_x \\ V_y \\ V_z \end{bmatrix} - \begin{bmatrix} 0 & 0 & \omega_\oplus \\ 0 & 0 & 0 \\ -\omega_\oplus & 0 & 0 \end{bmatrix} \begin{bmatrix} x \\ y \\ z \end{bmatrix} \tag{C.5}$$

Convert the velocity back to the up-east-north frame.

$$\begin{bmatrix} V_u \\ V_e \\ V_n \end{bmatrix} = \begin{bmatrix} \cos(-\phi) & 0 & -\sin(-\phi) \\ 0 & 1 & 0 \\ \sin(-\phi) & 0 & \cos(-\phi) \end{bmatrix} \begin{bmatrix} \cos(\theta) & \sin(\theta) & 0 \\ -\sin(\theta) & \cos(\theta) & 0 \\ 0 & 0 & 1 \end{bmatrix} \begin{bmatrix} V_x \\ V_y \\ V_z \end{bmatrix} \tag{C.6}$$

And finally convert the velocity back to spherical coordinates, taking care to recognize a

quadrant check is required.

$$\begin{bmatrix} \psi \\ {}^R\gamma \\ {}^R V \end{bmatrix} = \begin{bmatrix} \tan^{-1}\left(V_e/V_n\right) \\ \tan^{-1}\left(V_u/\sqrt{V_e^2 + V_n^2}\right) \\ \sqrt{V_e^2 + V_n^2 + V_u^2} \end{bmatrix} \tag{C.7}$$

The relative state vector is now:

$$\begin{bmatrix} r \\ {}^R V \\ \theta \\ \phi \\ {}^R\gamma \\ \psi \end{bmatrix} \tag{C.8}$$

Bibliography

[1] "Joint LRGPE - Virtual Industry Capability Call (VICC)." 8 September 2008
https://pixs.wpafb.af.mil/pixs_solicitation.asp?id=2324.

[2] "Falcon." 19 September 2008 http://www.darpa.mil/tto/programs/Falcon.htm.

[3] "Jets and Moon Rockets: 1957-1970; The Boeing Company ... Dynamic Soaring." 9
October 2008 http://www.boeing.com/history/narrative/n054boe.html.

[4] "OptControlCentre." 8 September 2008
http://www.optcontrolcentre.com/html/nlp_solvers.html.

[5] "Reusable Launch Vehicle." 8 September 2008
http://www.sti.nasa.gov/tto/spinoff1996/14.html.

[6] "STS-120 Shuttle Mission Imagery." 9 October 2008
http://spaceflight.nasa.gov/gallery/images/shuttle/sts-120/html/sts120-s-028.html.

[7] "X-Series Aircraft." 8 September 2008
http://www.edwards.af.mil/gallery/html_pgs/xseri4.htm.

[8] Bellman, Richard E. *Dynamic Programming.* Princeton: Princeton University Press,
1957.

[9] Betts, John T. *Practical Methods for Optimal Control using Nonlinear Programming.*
Philadelphia PA: Society for Industrial and Applied Mathematics, 2001. pp. 190.

[10] Blocker, W. D., D. R. Komar, M. K. Bradley and D. J. McCormick. "NGLT
Assessment of the Boeing FASST TSTO Air-breathing Vehicle Concept," in *39th
AIAA/ASME/SAE/ASEE Joint Propulsion Conference and Exhibit,* 2003.

[11] Bryson, Arthur E. *Dynamic Optimization.* Menlo Park CA: Addison Wesley
Longman, 1999. pp. 434.

[12] Bryson, Arthur E. and Y. Ho. *Applied Optimal Control; Optimization, Estimation, and
Control.* Waltham MA: Blaisdell Pub. Co, 1969. pp. 481.

[13] Cacuci, D. G., M. Ionescu-Bujor and I. M. Navon. *Sensitivity and Uncertainty Analysis.* Boca Raton Fla.: Chapman & Hall/CRC, 2003.

[14] Chilton, Kevin P., General. "Statement of General Kevin P. Chilton, Commander, United States Strategic Command Before the Strategic Forces Subcommittee, House Armed Services Committee on United States Strategic Command," 27 February 2008. http://armedservices.house.gov/pdfs/STRAT022708/Chilton_Testimony022708.pdf.

[15] Clausen, Jens. "Course 42111: Static & Dynamic Optimization." Course Slides. 17 September 2008 www2.imm.dtu.dk/courses/02711/OptCond.Rev.pdf.

[16] Gill, Philip E., W. Murray and M. H. Wright. *Practical Optimization.* London ; NY: Academic Press, 1981. pp. 401.

[17] Gockenbach, Mark S. "Introduction to Sequential Quadratic Programming." Course Notes. 5 December 2008 http://www.math.mtu.edu/~msgocken/ma5630spring2003/lectures/sqp1/sqp1.pdf.

[18] Harpold, J. C. and Graves, Claude A., Jr. "Shuttle Entry Guidance," *Journal of the Astronautical Sciences,* vol. 27, pp. 239-268, July-Sept. 1979.

[19] Henry, Gary N. *The Decision Maker's Guide to Robust, Reliable, and Inexpensive Access to Space.* Air War College (AU), Maxwell Air Force Base AL, Feb. 2003.

[20] Hicks, Kerry. *Introduction to Astrodynamic Reentry.* Unpublished textbook. 2007.

[21] Houchin, Roy F., II *U.S. Hypersonic Research and Development: The Rise and Fall of DYNA-SOAR, 1944-1963.* NY: Routledge, 2006.

[22] Huntington, Geoffrey T., D. A. Benson, J. P. How, N. Kanizay, C. Darby and A. V. Rao. "Computation of Boundary Controls Using a Gauss Pseudospectral Method," in *AAS/AIAA Astrodynamics Specialist Conference,* 2007.

[23] Jorris, Timothy R. *Common Aero Vehicle Autonomous Reentry Trajectory Optimization Satisfying Waypoint and No-fly Zone Constraints.* Air Force Institute of Technology (AU), Wright-Patterson Air Force Base OH, September 2007.

[24] Kay, W. D. "The X-15 Hypersonic Flight Research Program: Politics and Permutations at NASA." 8 September 2008 http://history.nasa.gov/SP-4219/Chapter6.html.

[25] Rao, Anil V. *User's Manual for GPOCS(c) Version 1.0: A Matlab(r) Implementation of the Gauss Pseudospectral Method for Solving Multiple-Phase Optimal Control Problems.* TOMLAB(TM), Gainesville FL 32607, June 2007.

[26] Rao, Anil V. *A History, Comparative Study, and Application of Pseudospectral Methods.* PowerPoint. 2008.

[27] Rao, Anil V. and K. A. Clarke. "Performance Optimization of a Maneuvering Re-entry Vehicle Using a Legendre Pseudospectral Method," in *AIAA Atmospheric Flight Mechanics Conference and Exhibit,* 2002.

[28] Richie, George. "The Common Aero Vehicle: Space Delivery System of the Future," in *AIAA Space Technology Conference & Exposition,* 1999.

[29] Ross, I. M. *A Beginner's Guide to DIDO (Ver. 7.3): A MATLAB(c) Application Package for Solving Optimal Control Problems.* Elissar, LLC, November 2007.

[30] Slotine, J. -. E. and W. Li. *Applied Nonlinear Control.* Englewood Cliffs NJ: Prentice Hall, 1991. pp. 459.

REPORT DOCUMENTATION PAGE

1. REPORT DATE *(DD-MM-YYYY)*	2. REPORT TYPE	3. DATES COVERED *(From - To)*

4. TITLE AND SUBTITLE

5a. CONTRACT NUMBER

5b. GRANT NUMBER

5c. PROGRAM ELEMENT NUMBER

6. AUTHOR(S)

5d. PROJECT NUMBER

5e. TASK NUMBER

5f. WORK UNIT NUMBER

7. PERFORMING ORGANIZATION NAME(S) AND ADDRESS(ES)

8. PERFORMING ORGANIZATION REPORT NUMBER

9. SPONSORING/MONITORING AGENCY NAME(S) AND ADDRESS(ES)

10. SPONSOR/MONITOR'S ACRONYM(S)

11. SPONSOR/MONITOR'S REPORT NUMBER(S)

12. DISTRIBUTION/AVAILABILITY STATEMENT

13. SUPPLEMENTARY NOTES

14. ABSTRACT

15. SUBJECT TERMS

16. SECURITY CLASSIFICATION OF:			17. LIMITATION OF ABSTRACT	18. NUMBER OF PAGES	19a. NAME OF RESPONSIBLE PERSON
a. REPORT	b. ABSTRACT	c. THIS PAGE			
					19b. TELEPHONE NUMBER *(Include area code)*